



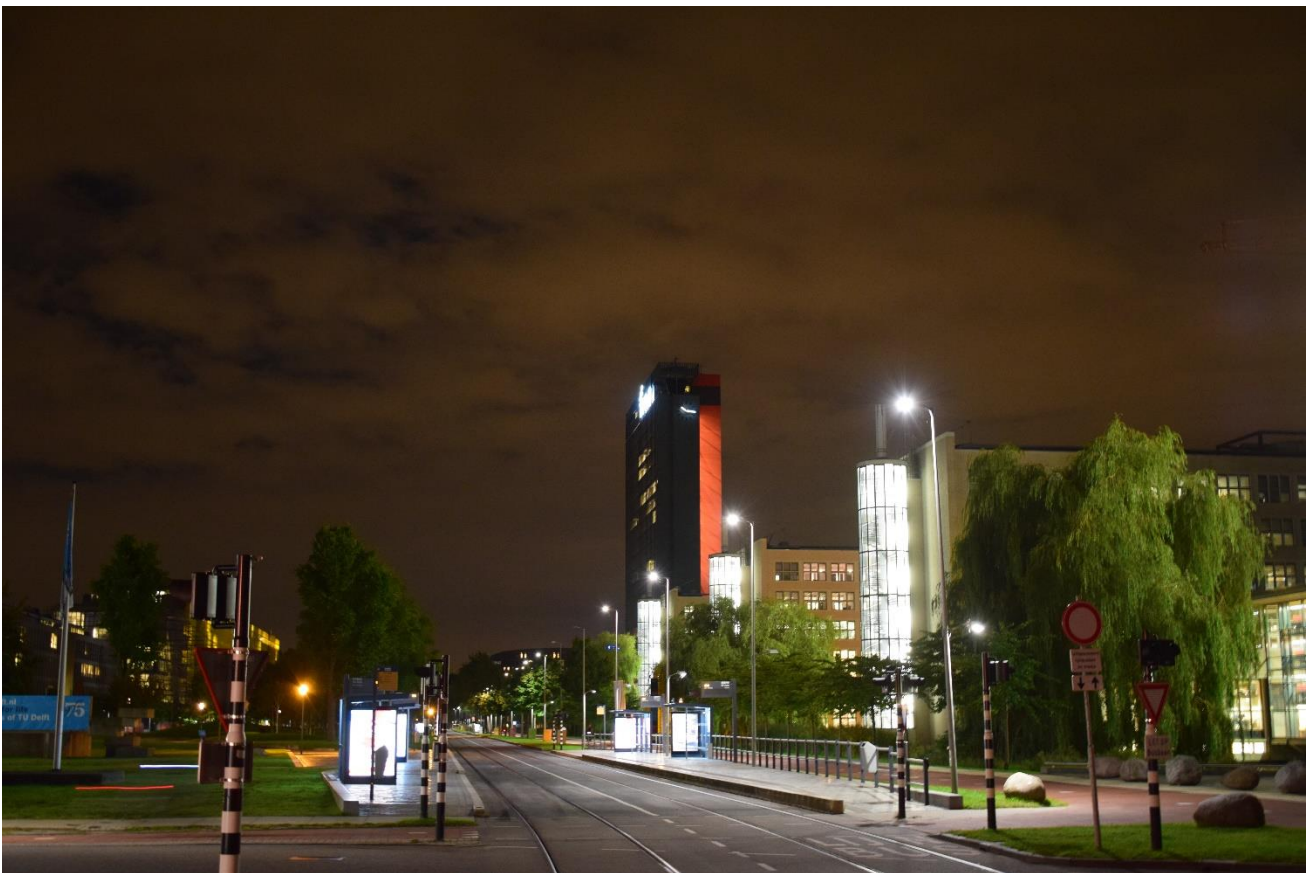
Master Thesis

Tie-Simplex Parameterization of Operator-Based Linearization for Isothermal Multiphase Compositional Flow In Porous Media

Author: **Geetha Krishna Choudary Konidala**

Advisor: **Denis. V. Voskov, TU Delft**

Supervisor: **Mark Khait, TU Delft**



Tie-Simplex Parameterization of Operator-Based Linearization for Isothermal Multiphase Compositional Flow In Porous Media

by

Geetha Krishna Choudary Konidala

to obtain the degree of **Master of Science in Petroleum Engineering and Geosciences**
from Department of Applied Earth Sciences
at the **Delft University of Technology**,
to be defended publicly on Wednesday October 31, 2018 at 10:00 AM.

Student number: 4627628
Project duration: Jan, 2018 – October, 2018
Thesis committee: Dr. Denis. V Voskov, TU Delft, Advisor
Prof Dr. William Rossen, TU Delft, Committee member
Dr. Anne Catherine Dieudonne, TU Delft, Committee member
Mark Khait, TU Delft, Supervisor

This thesis is confidential and cannot be made public until October 31, 2018.

An electronic version of this thesis is available at <http://repository.tudelft.nl/>.

Abstract

Compositional flow simulation is the best practise to model the complex enhanced oil recovery process. This involves solving highly coupled and non linear flow, transport equations. Interaction of components within different phases and the fluid interaction with rock properties makes it difficult to accurately predict the natural flow process in the reservoir. This demands for resolution models and accurate representation of flow process with realistic assumptions., which is quite challenging with conventional simulation.

The newly proposed Operator based linearization (OBL) approach handles the problem in a different way. Governing equations are regrouped using state and space operators. The state operators are computed at the nodes of uniform mesh in parameter space and multi- linear interpolation is performed during simulation. Uniformly distributed supporting points ignore the underlying physics leading to higher interpolation error around the phase boundary and demanding higher resolution to achieve the desired accuracy.

The objective of “Tie simplex parameterization of Operator-Based Linearization for Isothermal Multiphase Compositional flow in porous media” is to parameterize the compositional space by accounting the underlying physics. A set of tie lines captures the phase boundary in parameter space at given pressure and temperature. Tessellation is performed by extending the tie lines to the entire compositional space. The supporting points are assigned along the extended tie-lines according to manually designed heuristics. After that, the parameterized space is tessellated further using Delaunay triangulation, and barycentric interpolation is performed within each simplex.

The efficiency of the developed approach is demonstrated in comparison with the uniform parameterization using 1D displacement of compositional two-phase fluid. The convergence of non linear newton iterative solver is studied by applying the OBL framework with newly proposed interpolation and existing Multi-Linear interpolation framework.

Geetha Krishna Choudary Konidala
Delft, October 2018

Acknowledgement

Denis taught us a modelling course AES-1320 in my 1st year of masters and that motivated me to take up my thesis on Reservoir Simulation. I feel lucky to work on this amazing thesis, and happy for contributing my part to the next generation simulator Denis and Mark are developing. For the past 10 months, this work challenged me in many aspects and I learned during the process. Above all, this pulled me out of everything that was happening around me.

Denis is someone that every learner aspires for and Mark is the mentor that every student looks up to. They both created a comfortable space for me to work during my thesis. I thank my supervisor Mark for correcting the script and giving his valuable insights. Mark helped me in tuning my approach towards a problem, instrumental in shaping my thought process to a certain extent in both personal and professional capacity. Denis is always ready with ideas and different approaches during my thesis, his excitement for learning is something that struck deep in my mind. I thank his patience during the early days, I thoroughly enjoyed working on the basic OBL framework.

Every one of my batchmates can't forget FDP days. I thank Bill Rossen and the team for making it possible in giving us the best, yet intense learning experience for 6 weeks. Learning comes from multiple quarters, so does from friends. I observed people here, learned from them and had fun with them. My classmates are amazing, I enjoyed the quality time I spent with them and deeply cherished their presence. I carry forward some of the fond memories and their friendship.

This journey would not have been possible without the support I received from family and friends. My father has always encouraged me and provided abundant freedom in every possible situation. His strength inspired me to overcome many trying moments in this pursuit. My sister comforted my stay in Delft, by taking care of everything at home. She is the biggest X-factor. The innocence of my mother is always a delight to watch. A special gratitude goes to my aunts.

I'm deeply indebted to my friends back in India, their love and affection is always an additional boost for me. Without them, I couldn't have made into TU, Delft, they get a sizable amount of share. A special mention to Prof.K.V.Rao of JNTUK.

I always looked up to the act of Dashrath Manjhi and Friedrich Nietzsche's "He who has a Why can bear almost any How" quote.

Time truly flies, leaving behind memories and experiences. Delft chapter is the best phase I had for many reasons.

Signing off with satisfaction!

Dedicated

to

Ammamma

Contents

Acknowledgement	iii
	iv
List of Figures	vii
List of Tables	ix
Nomenclature	x
1 Introduction	1
1.1 Basic Motivation	1
1.2 Governing Equations	2
1.2.1 Phase Equilibrium	2
1.3 Molar Formulation	4
1.4 Operator Based Linearization	5
1.5 Iterative Solution Scheme	6
1.6 Interpolation Framework	7
1.7 Research Goals	7
2 Extrapolation of Non-Physical Supporting Points	8
2.1 Problem Statement	8
2.2 Extrapolation Technique	8
2.3 Results	9
2.3.1 Constant K-values representation	9
2.3.2 EOS-based representation	12
3 Interpolation Framework for Non-Uniform Mesh	14
3.1 Delaunay triangulation	14
3.1.1 Parameterization in Pressure and Composition	15
3.2 Interpolation Framework	15
3.2.1 Estimating Operators	16
3.2.2 Finding Derivatives	16
3.2.3 Derivative Plots	17
4 Adaptive Parameterization by Tie-Line Approach	20
4.1 Parameterization Scheme	20
4.1.1 Constant K-values parameterization	21
4.1.2 EOS-based parameterization	21
4.2 Spatial Distribution of Errors	23
4.3 Results	24
4.3.1 Constant K-values parametrization	24
4.3.2 EOS-based parametrization	25
4.3.3 Sensitivity Analysis	28
5 Validation of Tie-Simplex Parameterization	31
5.1 Transport Solver	31
5.1.1 Scheme of Solver	31
5.2 Validation	32
5.3 Accuracy of Solution	32
5.4 Nonlinear Convergence Study	33
5.5 Results	33
5.5.1 Three Component System	33
5.5.2 Four Component System	37

5.6 Performance of Tie-Simplex Parameterization	39
6 Conclusions and Discussion	40
Bibliography	42
A Appendix 1	44
B Appendix 2	45
B.1 Rock and fluid properties for OBL	45
B.2 Inputs of 1D reservoir simulation model	45
C Appendix 3	47
C.1 Geometric Constraint at Low Pressures	47
C.2 Derivatives Plots at Higher Resolution	48

List of Figures

2.1	Representation of supporting points (physical and non-physical) distributed uniformly in parameter space	9
2.2	Comparison of Euclidean error α before (left) and after (right) extrapolation for CO_2, nC_4, C_{10} at 56.6 bar with 4 resolution	10
2.3	Euclidean accumulation operator α before extrapolation (top left), after extrapolation (top right) and true operator (bottom centre) at 56.6 bar with 4 resolution	10
2.4	Comparison of Euclidean error β before (left) and after (right) extrapolation for CO_2, nC_4, C_{10} at 56.6 bar with 4 resolution	11
2.5	Euclidean accumulation operator β before extrapolation (top left), after extrapolation (top right) and true operator (bottom centre) at 56.6 bar with resolution 4	11
2.6	Comparison of error of Euclidean accumulation operator α for CO_2, nC_4, C_{10} before (left) and after (right) extrapolation at 56.6 bar with resolution 4	12
2.7	Euclidean accumulation operator α before extrapolation (top left), after extrapolation (top right) and true operator (bottom centre) at 56.6 bar with 4 resolution	12
2.8	Number of Newton iterations for bi-linear and barycentric interpolation for Model 1(left) and Model 2(right)	13
2.9	Euclidean accumulation operator β before extrapolation (top left), after extrapolation (top right) and true operator (bottom centre) at 56.6 bar with 4 resolution	13
3.1	Triangles satisfying empty circle criterion	14
3.2	Convex hull representing the physical domain for triangulation space for three component system	15
3.3	Representation of compositional planes along the pressure axis	15
3.4	Schematic representation of a simplex with query point R and barycentres of each vertex	16
3.5	Derivatives of accumulation term about $\{z_1, z_2\}$ on top and bottom respectively, using barycentric interpolation (left) and multi-linear interpolation (right) at 60 bar	18
3.6	Derivatives of flux term about $\{z_1, z_2\}$ on top and bottom respectively, using barycentric interpolation (left) and multi-linear interpolation (right) at 60 bar	18
3.7	Error in derivatives of α to z_1 (left) and z_2 (right) with the two interpolation schemes at 60 bar pressure	19
3.8	Error of derivatives β to z_1 (left) and z_2 (right) with the two interpolation schemes at 60 bar pressure	19
4.1	Ternary representation of parameterization scheme for constant K	21
4.2	Ternary representation of parameterization scheme for EOS case	22
4.3	Ternary representation of phase diagram for constant K values at 75 bar and 345° K	24
4.4	Euclidean operator plots of accumulation term α at 75 bar and 345° K	24
4.5	Euclidean error in accumulation operator at 75 bar for uniform mesh (left) adaptive(right) with 45 and 42 supporting points respectively	25
4.6	Euclidean operator plots of accumulation term β at 75 bar and 345° K	25
4.7	Euclidean error in flux operator at 75 bar for uniform (left) adaptive(right) mesh with 45 and 42 supporting points respectively	25

4.8 Ternary representation of phase diagrams at pressures 30, 65, 100 bar at 345° K for fully EOS case	26
4.9 Euclidean operator plots of accumulation term α at 30, 65, 100 bar and 345° K	26
4.10 Error in accumulation operator using adaptive parameterization at 30, 65, 100 bar for composition CO_2, NC_4, C_{10}	27
4.11 Error in accumulation operator using uniform parameterization at 30, 65, 100 bar for composition CO_2, NC_4, C_{10}	27
4.12 Euclidean operator plots of flux term β at 30, 65, 100 bar and 345° K	27
4.13 Error in flux operator using adaptive parameterization at 30, 65, 100 bar for composition CO_2, NC_4, C_{10}	27
4.14 Error in flux operator using uniform parameterization at 30, 65, 100 bar for composition CO_2, NC_4, C_{10}	28
4.15 Variation of maximum error in accumulation term for uniform and adaptive mesh at 30, 75, 120 bar respectively	28
4.16 Variation of maximum error in flux term for uniform and adaptive mesh, at 30, 75, 120 bar respectively	29
4.17 Variation of maximum error with refinement in accumulation operator α for uniform and adaptive mesh at 30, 75, 120 bar respectively	29
4.18 Variation of maximum error with refinement in flux operator α for uniform and adaptive mesh, at 30, 75, 120 bar respectively	30
5.1 Displacement profile of 1D simulation for Model 1 on left and Model 2 on right at resolutions 2,4,8,16 for uniform mesh using barycentric interpolation	32
5.2 Error of unknowns at every grid block in the reservoir model 1 (on left) and solution from tie-simplex parameterization (on right) for resolution 16	34
5.3 Average error in pressure and composition for each grid block for longer and shorter models at resolution 16, 64, 128	34
5.4 Number of Newton's iterations of barycentric interpolation and multi-linear interpolation with uniform mesh for Model 1 (on left) and Model 2 (on right) for three component system with constant K values	35
5.5 Number of Newton's iterations of barycentric interpolation with uniform mesh and adaptive mesh for Model 1 (on left) and Model 2 (on right) for three component system with constant K values	35
5.6 Average error in pressure and composition for each grid block for longer and shorter models at resolution 16,64,128 for three component fully EOS case	36
5.7 Number of Newton's iterations for barycentric and multi-linear interpolation for Model 1 (left) and Model 2 (right) for three component fully EOS case	37
5.8 Number of Newton's iterations of barycentric interpolation with uniform mesh and multi-linear interpolation for Model 1 at Δt_{max} of 1 day	37
5.9 Number of Newton's iterations for multi-linear and tie-simplex parameterization for model 1(left) and model 2(right) for four component constant K values	38
5.10 Number of Newton's iterations for barycentric interpolation and multi-linear interpolation for Model 1 (on left) and Model 2 (on right) for four component fully EOS case	38
C.1 Ternary representation of parameterization scheme for 20 bar pressure	47
C.2 Ternary representation of parameterization scheme for 20 bar pressure	48
C.3 Derivatives of α about z_1 (on top) and about z_2 (bottom) using tie-simplex (left) and multi-linear (right) interpolation for Fully EOS case at resolution 100	48
C.4 Derivatives of β about z_1 (on top) and about z_2 (bottom) using tie-simplex (left) and multi-linear (right) interpolation for fully EOS case at resolution 100	49

List of Tables

1.1	Unknowns of nonlinear formulation	5
2.1	Average error before and after extrapolation for constant K value case	11
2.2	Average error before and after extrapolation for EOS case	13
4.1	Number of supporting points in uniform and adaptive mesh for EOS case	26
5.1	Injection and production conditions for 3 component fluid system	33
5.2	Error of unknowns in tie-simplex parameterization in comparison with multi-linear interpolation for constant-K	34
5.3	Average number of supporting points for uniform and adaptive mesh for constant K values	36
5.4	Error of unknowns in tie-simplex parameterization in comparison with multi-linear interpolation for fully EOS case	36
5.5	Injection and production conditions for 4 component fluid system	38
5.6	Comparison of interpolation time of tie-simplex parameterization before and after initializing derivatives	39
B.1	Rock and fluid properties considered for OBL framework	45
B.2	Inputs parameters for 1D system for three and four component system	45
B.3	Input parameters for 1D simulation	46
B.4	K values for three and four component system	46

Nomenclature

Governing Equation

n_p	Number of Phases
n_c	Number of Components
p	Pressure
T	Temperature
z	Total composition
ρ_{cj}	Phase density of component c
s_{cj}	Phase saturation of component c
u_j	Darcy phase velocity
K_T	Absolute Permeability
k_{rj}	Phase relative permeability
μ_j	Phase viscosity
f_c	Fugacity of component c
v_j	Phase fraction

Phase Computations

K	Equilibrium ratios
p_c	critical pressure
T_c	critical temperature
w	Accentric factor
a	Attraction parameter
b	Repulsion Parameter

Algebraic Equation and OBL

ω	State dependent variable
ξ	space dependent variable
T	Transmissibility
V	Volume of grid block
α_c	Accumulation operator for component c
β_c	Flux operator for component c
r	Residual vector
J	Jacobian matrix

Barycentric Interpolation

γ	Barycentric Coordinates
R	Operators on vertex of simplex

1

Introduction

Oil and gas industry has evolved from the easy oil days to the fields which demand the complex application of science and engineering. The art of reservoir engineering evolved over the years, with the purpose of managing and producing hydrocarbons in the most effective way possible. The classical reservoir engineering mostly dealt with the analytic approach for solving the flow equations related to the reservoir. The age-old fields which involve complex physical processes, demands numerical solvers to perform computations. Finite difference methods laid the foundation for solving the equations governing a mathematical model of the reservoir, which eventually transfigured into a separate entity called “Reservoir Simulation”. Reservoir simulation deals with solving partial differential equations governing multiphase multicomponent flow in porous media. This is the best available method to quantify the uncertainty and risk associated with underground petroleum reservoirs (Aziz, 1979).

Two important characteristics of petroleum reservoirs are the nature of rock and of the fluids filling it. Fluid modeling is classified as flow with or without mass transfer between phases depending on undergoing recovery mechanisms. The complexity of fluid modeling is associated with the distribution of phase and composition across the chemical species present in the fluid system. This arises during the Enhanced Oil Recovery (EOR) stage of field development. An equation of state (EOS) compositional model was developed (Coats et al., 1980) for analyzing the phase distribution and its behavior in the reservoir. Based on the fluid sampling and PVT analysis (Nagarajan et al., 2006), different models like *black oil*, *volatile oil*, *compositional* models evolved for studying EOR, these models differ in the type of fluids they constitute, density and viscosity. Out of all, the compositional model has gained a significance because during EOR, the phase composition varies significantly within the reservoir and the injected fluids are different from the fluids already present in the reservoir, which is be effectively represented and modeled using compositional model. The guidelines for choosing the type of fluid model for gas reservoirs is discussed in detail by Fevang et al. (2000)

1.1. Basic Motivation

More accurate reservoir models are needed to study the complex underlying physics and uncertainties associated with the geology of reservoir. Conventional simulation faces challenges from multiple quarters, thereby making an accurate representation of the reservoir model and the computational efficiency of the simulator mutually exclusive. The difficulties arise in the form of accurate representation of physics, high-resolution models, the efficiency of linear solvers etc. In addition, numerical schemes introduce nonlinearity to the system of equations due to spatial and temporal approximations. Compositional models exhibit a strong coupling between the flow and transport of compositional changes, thereby making it expensive to execute the reservoir models with accurate representation.

Linearization is required to solve the nonlinear nature of the flow and transport problems

in porous media. A new linearization approach called Operator-Based Linearization (OBL) is proposed in pursuit of developing an efficient reservoir simulator by Voskov (2017). This approach reduces the nonlinearity of the problem using piece-wise multi-linear interpolation. The accuracy of the constructed approximation is driven by the density of supporting points in a given domain. The advantages of this approach were demonstrated by modeling the isothermal compositional transport for oil reservoirs with buoyancy (Khait et al., 2018b) and for geothermal applications (Khait and Voskov, 2018), for low enthalpy processes (Khait and Voskov, 2016). This method has an advantage of treating the physics terms separately and modeling fluid flow through porous media by considering an approximate physical representation with control over accuracy compromise.

1.2. Governing Equations

Isothermal multicomponent multiphase flow in porous media can be described using component material balance, momentum, and phase equilibrium equations. The mathematical description of fluid flow is based on the principle of mass conservation (mass balance), i.e., that the accumulation of mass in some domain is exactly balanced by the mass flowing through the boundary of the domain. Here, presence of sources/sinks in the the domain is neglected:

Rate of change of mass in a control volume = Accumulation of mass.

$$\frac{d}{dt} \left(\phi \sum_{j=1}^{n_p} x_{cj} \rho_j S_j \right) + \nabla \cdot \sum_{j=1}^{n_p} x_{cj} \rho_j u_j = 0, c = 1, \dots, n_c. \quad (1.1)$$

The components are distributed in fluid phases, e.g., oil, gas and water phases. Actually, fluid flow is characterized by the flow of phases rather than the flow of the individual components. In the above equation, Darcy's law is the relation between the gradient of the potential of a phase j and the phase volumetric flow rate u_j ,

$$u_j = - \left(K_T \frac{k_{rj}}{\mu_j} (\nabla p_j - \gamma_j \nabla d) \right), j = 1, \dots, n_p, \quad (1.2)$$

where K_T is the permeability tensor, and k_{rj} , μ_j and p_j are the relative permeability, viscosity and pressure of phase j respectively, γ_j represents the gravity term and d indicates the vector of depth.

1.2.1. Phase Equilibrium

The species in fluid system undergo mass transfer between phases, which is characterized by the variation of mass distribution of each component in the oil and gas phase. These two phases are assumed to be in a simultaneous phase equilibrium state. Under this assumption, the compositions of phases formed at a particular location in the porous media are determined by p , T and overall composition z . A multiphase flash procedure is performed for a given composition in each grid cell to solve the individual composition. Having completed the flash calculation in a cell, components compositions x_{cj} and phase molar fractions v_j are found.

Thermodynamic equilibrium is mathematically represented by equating the fugacity (or chemical potential) of components in the oil and gas phase.

$$f_{c1}(p, T, x_1) - f_{cj}(p, T, x_j) = 0, \quad (1.3)$$

Thermodynamic flash equilibrium calculation involves the set of thermodynamic local mass balance and constraint equations as listed below.

$$z_c - \sum_{j=1}^{n_p} v_j x_{ij} = 0, \quad i = 1, 2, 3, \dots, n_c \quad (1.4)$$

$$\sum_{c=1}^{n_c} (x_{i1} - x_{ij}) = 0, \quad j = 2, \dots, n_p \quad (1.5)$$

$$\sum_{j=1}^{n_p} v_j - 1 = 0. \quad (1.6)$$

$$Kx_{i1} = x_{ij} = 0, \quad i = 1, \dots, n_c \text{ and } j = 2, \dots, n_p \quad (1.7)$$

The above 1.3 to 1.4 equations give component distribution over phases for a given overall molar composition Z_c . And 1.7 mentions the relation between vapor and liquid compositions.

$$g(V_j) = \sum_{i=1}^{n_c} \frac{z_i(1 - K_i)}{V(K_i - 1) + 1} = 0, \quad i = 1, 2, \dots, n_c \quad (1.8)$$

The phase fraction v_p is obtained from phase saturation and densities:

$$v_p = \frac{S_p \rho_p}{\sum_i S_i \rho_i} \quad i = 1, 2, \dots, n_p \quad (1.9)$$

Phase modelling is done by two methods i.e. Constant-K value method and Fully-EOS method.

Constant K Values

Equilibrium ratios (K values) define the relation between the liquid and gas phase composition of each component. The constant K values are dependent on pressure p and temperature T (Bolling et al., 1987), but weakly dependent on composition. The condition of equality in fugacity is bypassed at equilibrium, which establishes a linear dependence between liquid and vapor fractions. So the two-phase region is enclosed between a set of two straight lines, rather than a closed enclosure. A critical point is never observed with constant K values. The Rachford-Rice equation (Rachford Jr et al., 1952) is solved using K values for solving thermodynamic equilibrium.

The above equation is solved using bi-section method to obtain V , which lies between the two asymptotes defined by minimum and maximum K values $\frac{1}{(1 - K_{min})} < V < \frac{1}{(1 - K_{max})}$. The compositions of liquid and vapor are calculated as follows

$$x_i = \frac{z_i}{1 + V(K_i - 1)} \quad (1.10)$$

$$y_i = K_i x_i \quad (1.11)$$

where V is vapor fraction, z_i is composition of each component, x_i and y_i represents mole fraction of component i in liquid and vapor phase respectively.

Fully EOS

In EOS based flash, K values are strongly dependent on composition. Introduction of fugacity in flash calculations induces the nonlinearity, thereby making it computationally expensive. But the accuracy of phase distribution is better than constant K value case. Out of different cubic equation of states, Peng Robinson Equation of State (Peng and Robinson, 1976) is used in petroleum reservoir simulation due to applicability to the wide range of pressures. The flash procedure is mentioned below:

1. Make an initial guess of K values. When the guess of K values are far from the equilibrium solution, the procedure might not converge. When the guess of the K-values is near the equilibrium solution, the procedure will converge rapidly. Wilson equation (an empirical correlation) gives the good estimates of K values.

$$K_i = \frac{x_{i,g}}{x_{i,o}} = \frac{p_{c,j}}{p} \exp\left[5.37\left(1 + w_i\left(1 - \frac{T_c}{T}\right)\right)\right], \forall i = 1, \dots, n_c \quad (1.12)$$

2. Once the K -values for each component are specified, the Rachford-Rice equation 1.8 is used to estimate the phase mole fractions. A simple material balance on each component 1.4 gives overall composition z_i . Equation 1.8 is solved using the iterative procedure, where the new value of the liquid mole fraction is determined when the convergence criterion is met.
3. The EOS parameters for Peng-Robinson (e.g., am and bm) are determined. The critical temperatures T_{tc} , pressures P_{pc} , and acentric factors ω_i for each component are needed to calculate these parameters.
4. Fugacity of the components in different components is determined using the following relation.

$$\log \frac{f_{kl}}{x_k p} = \frac{b_k}{b} (Z - B) - \frac{A}{\sqrt{2}B} \left(\frac{2 \sum_j x_j a_{jk}}{a} - \frac{b_k}{b} \right) \log \left(\frac{Z + (\sqrt{2} + 1)B}{Z - (\sqrt{2} - 1)B} \right) \quad (1.13)$$

5. K values for next iterations are updated with fugacity values of phases

$$K_i^m = K_i^{m-1} \frac{f_{i,o}^{m-1}}{f_{i,g}^{m-1}} \quad (1.14)$$

where m represents SSI iteration number.

1.3. Molar Formulation

For n component two-phase isothermal system, there are n equations expressing the conservation of mass of n components in different phases and $n + 1$ secondary equations corresponding to equality of fugacity between phases and saturation constraint. In total, this system needs $2n + 1$ equations (unknowns) to get solved at each grid block in the conventional simulation. Because the $n + 1$ constraint equations for a block involves unknowns only in the given block, they can be used to eliminate $n + 1$ secondary variables from block's n primary or conservation equations. Thus, in each block, n unknowns of primary equations are needed to be considered in the discussion of model formulation. The primary variables for solving the system is chosen from many available variables: phase composition, overall mole fraction, saturation etc.

Different formulations are available for solving system of governing equations, out of which, natural (phase-based) and molar (mass-based) formulation are widely used. They differ in the choice of primary variables (Aziz and Wong, 1989) and phase behavior computations during nonlinear convergence. In the natural formulation (Coats et al., 1980), pressure, saturation and compositions of components in phases are considered as primary unknowns, whereas in

the molar formulation (Acs et al., 1985), pressure and overall molar fractions of components are primary unknowns. The number of unknowns for n_c component n_p phase system is given in below table.

Table 1.1: Unknowns of nonlinear formulation

Formulation	Unknowns	Number of unknowns
Natural	p	1
	s_p	$n_p - 1$
	x_{cp}	$n_p(n_c - 1)$
Natural	p	1
	z_c	$n_c - 1$

1.4. Operator Based Linearization

In the conventional simulation, discretized governing equations are solved using Newton iterative method at every time step, making phase equilibrium calculations mandatory in each grid block for every nonlinear iteration. In the OBL approach, equation 1.1 are regrouped using space and state-based operators, thereby facilitating us treat the physics of the problem separately. Space based operator is composed from heterogeneous reservoir properties, such as porosity, permeability tensor etc, which do not depend on primary unknowns. State-based operator describes the underlying physics, which are mainly the fluid properties, fully defined by state in a given grid block. The coefficients of equations are defined as a function of spatial coordinates ξ and ω .

- State operators are
 - $k_{rj}(\omega)$ - Relative permeability,
 - $\rho_j(\omega)$ - Density,
 - $S_j(\omega)$ - Saturation,
 - $x_{cj}(\omega)$ - Mole-fraction of component c in phase j,
 - $\mu_j(\omega)$ - Phase viscosity.
- Space operators are
 - $K(\xi)$ - Permeability tensor,
 - $\phi(\xi)$ - Porosity,
 - $u_j(\omega, \xi)$ - Phase velocity.

While regrouping, the conservation equations 1.1 are represented in algebraic form in terms of the state and space operators as

$$r_c(\xi, \omega) = a(\xi)(\alpha_c(\omega) - \alpha_c(\omega_n)) - \sum_l \beta_c^l(\omega) b^l(\xi, \omega) = 0 \quad (1.15)$$

state variables

$$\alpha_c(\omega) = (1 + c_r(p - p_{ref})) \sum_j x_{cj} \rho_j S_j \quad (1.16)$$

$$\beta_c(\omega) = \sum_j x_{cj} \rho_j \frac{k_{rj}}{\mu_j} \quad (1.17)$$

space variables

$$a(\xi) = V(\xi) \phi_0(\xi), \quad (1.18)$$

$$b(\xi, \omega) = \Delta t T^{ab}(\xi)(p^b - p^a), \quad (1.19)$$

Here a depends on the spatially distributed property (porosity ϕ and block volume) and b depends on transmissibility (block geometry and permeability related). State operators α and β depend on rock and fluid property. Accuracy in the space variables $a(\xi)$, $b(\xi, \omega)$ is controlled by spatial and temporal resolution.

The parameter space domain is uniformly parameterized and state-based operators α_c and β_c are calculated at the nodes of the resulting grid. These calculations are stored in a table form and are called supporting points.

During simulation, these operators at any arbitrary point in the domain are approximated by performing multi-linear interpolation. So, the accuracy of α_c and β_c representation depends on the number of supporting points in parameter space. These arbitrary points are referred to as query points. The dimensionality of parameter space depends on the type of nonlinear formulation used for solving the system. Since we are employing molar formulation, for isothermal problem, the parameter space is constituted by pressure and $n_c - 1$ overall molar compositions, resulting in n_c dimensions depending on the number of components. Based on the dimension of parameter space, set of adjacent supporting points constitutes an interpolation body e.g, square for three-dimensional parameter space, cube for 4D parameter space.

Flash equilibrium computations are needed only during preprocessing stage, when supporting points are computed. For query points, this is replaced by interpolation scheme during simulation making it iteration free procedure from flash calculations. By that, OBL enjoys supreme computational efficiency than the conventional compositional simulator, as mentioned by Voskov (2017).

1.5. Iterative Solution Scheme

A time-dependent, nonlinear coupled system needs a stable and efficient numerical scheme to solve the discretized equation. Several solution techniques like explicit, adaptive implicit and fully implicit solvers are available. The classical explicit methods find its frequent usage in reservoir simulation. But the solution is stable only at relatively short time steps dictated by CFL number. Rapidly changing fluxes even in a single grid block will affect the stability of the entire solution. So, enormous computations are needed to simulate a long time period in field-scale model, and thus explicit methods are not used for this strong nonlinear problem. The robust Implicit solver is preferred for this type of solutions.

The algebraic system of nonlinear equations 1.15 can be reduced to a linear form by constructing a Jacobian matrix with unknowns $(p, z_1, \dots, z_{n_c-1})$. A robust, fully implicit solution technique usually based on Backward Euler scheme Butcher (2016) is used for solving the equation 1.15 numerically. The overall composition in each grid-cell varies with time. This is due to cell-to-cell fluxes which arise from the pressure difference. The nonlinear system is solved using the iterative Newton-Raphson method until a specified convergence criterion is met. Each Newton iteration requires

- Linearizing of the discretized governing equations
- solving the algebraic equation until convergence.
- Updating nonlinear unknowns using linear solution.

$$J_{ic} = \frac{dF_i}{d\eta_c}, \eta = [p, z_1, z_2, \dots, z_{n_c-1}] \quad (1.20)$$

$$J^k \cdot \delta y^k = -r^k \quad (1.21)$$

The correction is then added to solution vector y as an update to nonlinear unknowns.

$$y_{new} = y_{old} + \delta y^k \quad (1.22)$$

1.6. Interpolation Framework

The current OBL framework uses multi-linear interpolation proposed by ?, within a hypercube (an n dimensional analog of a square) in parameter space. In uniform parameterization, the parameter space is a collection of hypercubes stacked together, each one comprising of 2^{nc} supporting points along the edges.

After discretizing the parameter space into N equal intervals i.e. pressure and composition into $[P_1, P_2, \dots, P_N], [Z_{1,2}, \dots, Z_N]$, an interpolant function $f_{i,j} = f(P_i, Z_i)$ is created, where f is α_1 to nc , β_1 to nc . For a given query point $[p, z]$, where $p \in [P_i, P_{i+1}]$ and $z \in [Z_j, Z_{j+1}]$ linear interpolation is performed as follows,

$$p_i = \frac{p - P_i}{P_{i+1} - P_i}, \quad z_j = \frac{z - Z_j}{Z_{j+1} - Z_j} \quad (1.23)$$

$$F_f = (1 - z_j)[(1 - p_i)f_{i,j} + p_i f_{i+1,j}] + z_j[(1 - p_i)f_{i,j+1} + p_i f_{i+1,j+1}] \quad (1.24)$$

and the derivatives as follows

$$\frac{\partial F_f}{\partial p} = \frac{(1 - z_j)[f_{i+1,j} - f_{i,j}] + z_j[f_{i+1,j+1} - f_{i,j+1}]}{P_{i+1} - P_i} \quad (1.25)$$

$$\frac{\partial F_f}{\partial z} = \frac{(1 - p_i)[f_{i,j+1} - f_{i+1,j}] + p_i[f_{i+1,j+1} - f_{i+1,j}]}{Z_{j+1} - Z_j} \quad (1.26)$$

In the course of simulation, an update in nonlinear unknown is based on the solution from linear system. There are different chopping procedures exist for non linear update. We use Appleyard chop (GeoQuest, 2009), which corrects the update in saturation locally according to the end points of relative-permeability function.

1.7. Research Goals

The accuracy of OBL framework depends on resolution: piece-wise multi-linear approximation of state operators introduces an error. However, due to their nonlinearity, the spatial distribution of the error is varying across the parameter space. Uniform parameterization distributes the supporting points at equal distances in parameter space, without accounting for the underlying physics requiring more supporting points to achieve certain accuracy. In addition, for fluid systems with more than 2 components, uniform parameterization leads to the necessity to compute values of space operators for supporting points lying outside of physical domain.

Even though the latter problem can be addressed by accurate extrapolation of operator value, as was shown in Chapter 2, there is more elegant solution addressing both problems.

Non-uniform parameterization of parameter space by considering the phase boundary and positioning the supporting points along the boundary can reduce the maximum error in the domain with the same amount of supporting points, while nonphysical supporting points do not arise by definition. For adaptive parameterization, we make use of Compositional Space Parameterization (CSP) idea proposed for flow simulation by Voskov and Tchelepi (2009), which is applied to multi contact miscible system (Voskov et al., 2009b) and for immiscible miscible displacement problems (Voskov et al., 2009a). This method is demonstrated by Zaydullin et al. (2013), in which the thermodynamic phase-behavior is represented in the tie-simplex space as a function of pressure, composition, and phase fractions. The parameterized space is tessellated by Delaunay triangulation, thus all the operator values become a piece-wise linear function in the tie-simplex space. Since the simplexes are nonuniform in compositional space, barycentric interpolation framework is adopted in our research.

In a simplistic sense, this research is an incorporation of CSP strategy and the suitable interpolation framework to OBL approach and validating the newly developed approach with one-dimensional compositional transport solver.

2

Extrapolation of Non-Physical Supporting Points

For compositional system with more than two components, only half of the points in parameter space is valid due to composition constraint $\sum_{i=1}^{nc} z_i = 1$. This indicates the supporting points used in multi-linear interpolation from non-physical space are invalid, so operator values can not be computed there. In the existing OBL framework, operator values are computed at the closest physical supporting point instead, and then simply assigned to the non-physical point. However, this method introduces additional error. This chapter describes a more accurate approach for computation of non-physical supporting points along the boundary of physical space to minimize the approximation errors. This approach is tested for three component system.

2.1. Problem Statement

Uniformly distributed supporting points form a set of hypercubes which are tessellated in parameter space. The operator values at each query point are determined by multi-linear interpolation. The interpolation bodies lying on non-physical space completely are not used in interpolation, but the ones which share both physical and non-physical space can be employed. Interpolation strategy in existing OBL framework is designed in such a way that the auxiliary function values at the midpoint of all the hypercube along the diagonal are assigned to the vertices of the corresponding hypercube in the non-physical region. This is illustrated in the figure 2.1.

The dots, highlighted in black, represent the supporting points in physical space, while in orange color, non-physical supporting points are shown. Squares highlighted in red shares both physical and non-physical part of the space. The operator values determined at D_1, D_2, D_3, D_4 are assigned to the points NP_1, NP_2, NP_3, NP_4 . This induces error due to inconsistency between weights of the supporting points and its operator values in non-physical points NP_1, NP_2, NP_3, NP_4 .

2.2. Extrapolation Technique

An extrapolation technique is devised to have accurate interpolated operator values, when query point matches with D_1, D_2, D_3, D_4 points by construction. The operator values at non-physical supporting points are found using extrapolation equation.

$$f_{i+1/2, j+1/2} = (f_{i,j} * w_{i,j}) + (f_{i+1,j} * w_{i+1,j}) + (f_{i,j+1} * w_{i,j+1}) + (f_{i+1,j+1} * w_{i+1,j+1}), \quad (2.1)$$

where $f_{i+1/2, j+1/2}$ represents the operator values at the centre of interpolation body (D_1, D_2, D_3 in fig: 2.1) , $f_{i+1, j+1}$ corresponding to the auxiliary function at non-physical points, w cor-

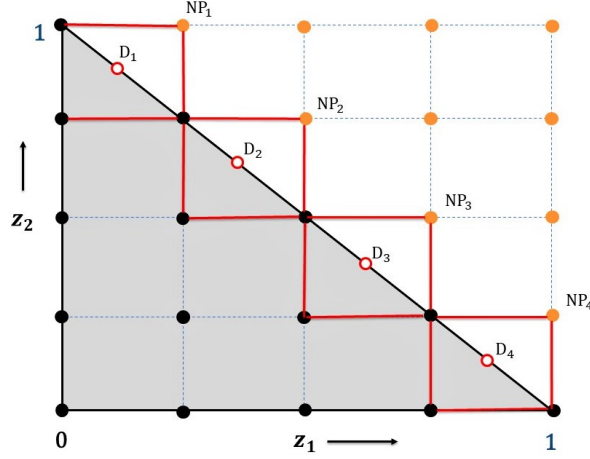


Figure 2.1: Representation of supporting points (physical and non-physical) distributed uniformly in parameter space

responds weights of the auxiliary function f with respect to midpoint of each interpolating body along the diagonal.

For three component system with resolution N , extrapolation is performed for $N - 1$ supporting points $NP_1, NP_2, \dots, NP_{N-1}$. The effect due to incoherent operator values at non-physical supporting points can be confirmed by performing error analysis between the interpolated and accurately determined operator value conventionally. The effect of the extrapolation scheme is quantitatively demonstrated by calculating the average error over the physical space:

$$Error = \frac{|f(true)_\Omega - f(Interpolated)_\Omega|}{\max(f(true)_\Omega)}, \quad (2.2)$$

where f represents the accumulation and flux operator values.

2.3. Results

Three component fluid system CO_2, nC_4, C_{10} is considered between 20 and 130 bars at $345^\circ K$. Parameter space $[p, z_1, z_2]$ is uniformly parameterized into $n * n^2$ supporting points, n being the number of equal intervals for parameterization.

Error analysis is performed at pressure 56.6 bar for three different resolution 4, 16, 64 and the error plots for resolution 4 is presented below. Since the pressure 56.6 bars corresponds to the base pressure, the error plots presented below has no error due to the pressure interpolation. The error is minimum in the area proximate to supporting points and shows absolute zero for the supporting point at base pressure. Results for constant K values and EOS cases are presented below.

2.3.1. Constant K-values representation

In the below figure 2.2, error is more concentrated close to the physical boundary. This is can be explained by examining the operator α for different cases in fig 2.3. A shape of concavity is observed in plot α (left top) without extrapolation when compared with the operator value after extrapolation (top right). Extrapolation strategy restores the shape of α operator plot after extrapolation almost resembles the convex operator shape, which leads to the reduction of maximum error in fig 2.2. The error is reduced substantially since the variation of operator α is smooth and due to the absence of nonlinear/abrupt changes in the operator. After extrapolation, the error associated is only due to spatial distribution and nonlinear variation in operator, which can be controlled by resolution.

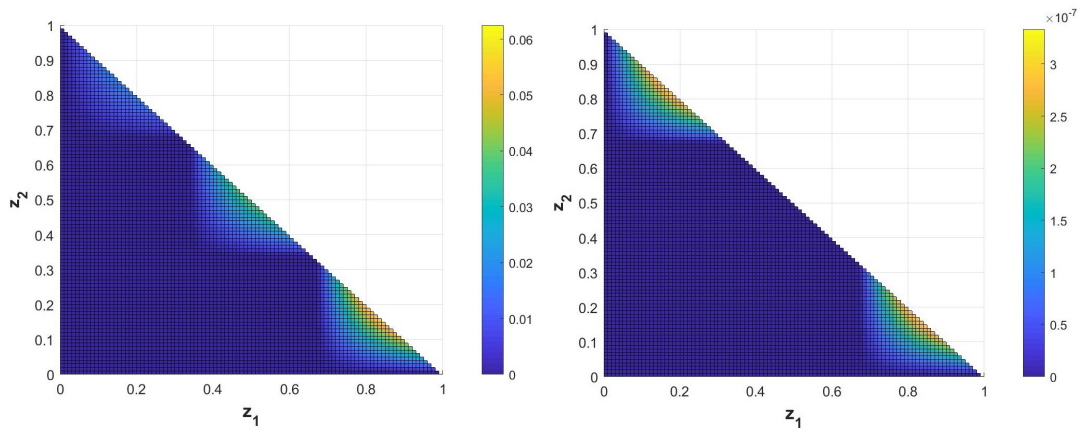


Figure 2.2: Comparison of Euclidean error α before (left) and after (right) extrapolation for CO_2, NC_4, C_{10} at 56.6 bar with 4 resolution

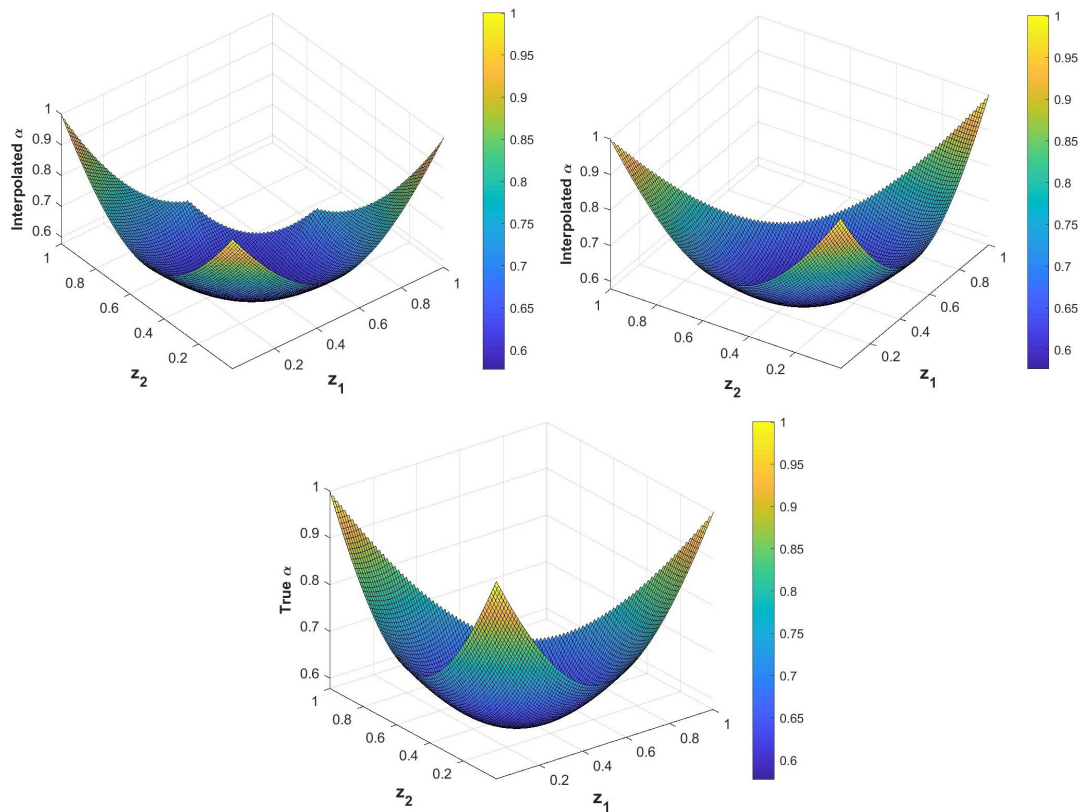


Figure 2.3: Euclidean accumulation operator α before extrapolation (top left), after extrapolation (top right) and true operator (bottom centre) at 56.6 bar with 4 resolution

Unlike the error plot of α , operator β has both the error associated with nonlinearity and the error due to the mismatched shape of concavity close to the boundary. The difference is clearly observed between left and right plots in fig 2.4. In order to exactly represent the nonlinearity operators like β , this linearization approach needs high resolution.

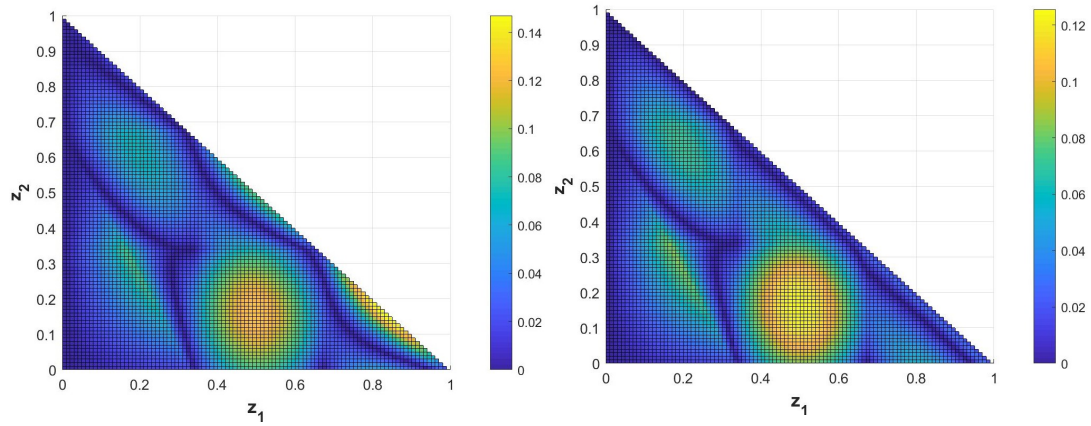


Figure 2.4: Comparison of Euclidean error β before (left) and after (right) extrapolation for CO_2, nC_4, C_{10} at 56.6 bar with 4 resolution

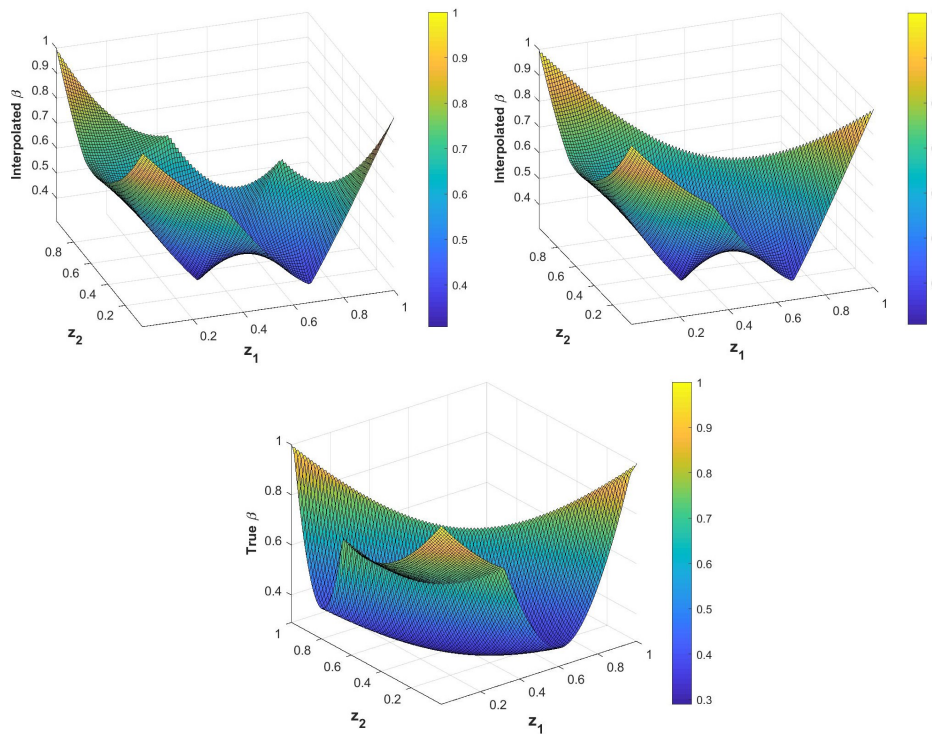


Figure 2.5: Euclidean accumulation operator β before extrapolation (top left), after extrapolation (top right) and true operator (bottom centre) at 56.6 bar with resolution 4

The error, averaged over entire physical space, is presented below.

Table 2.1: Average error before and after extrapolation for constant K value case

Operator	Resolution	Before Extrapolation	After Extrapolation
α	4	8.86×10^{-3}	4.41×10^{-8}
	16	7.27×10^{-4}	1.40×10^{-8}
	64	9.3×10^{-5}	1.06×10^{-8}
β	4	0.049	0.037
	16	0.019	0.013
	64	4.20×10^{-4}	3.26×10^{-4}

2.3.2. EOS-based representation

In the figure 2.6, the error concentrated close to the physical space is a combination of error due to the nonlinearity of α and due to inconsistency in operator value at the non-physical supporting point. In the region corresponding to the high error in fig 2.6 (left), almost linear trend is observed in the operator α in without extrapolation strategy, compared to the true operator value.

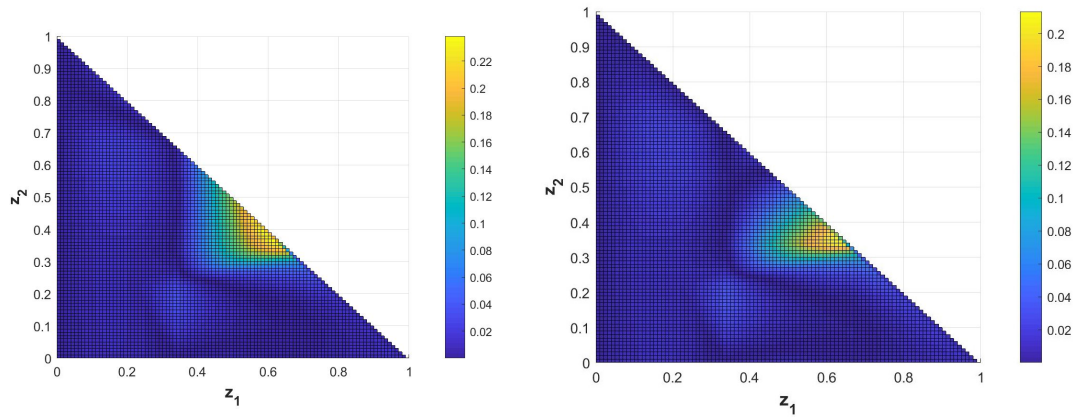


Figure 2.6: Comparison of error of Euclidean accumulation operator α for CO_2, nC_4, C_{10} before (left) and after (right) extrapolation at 56.6 bar with resolution 4

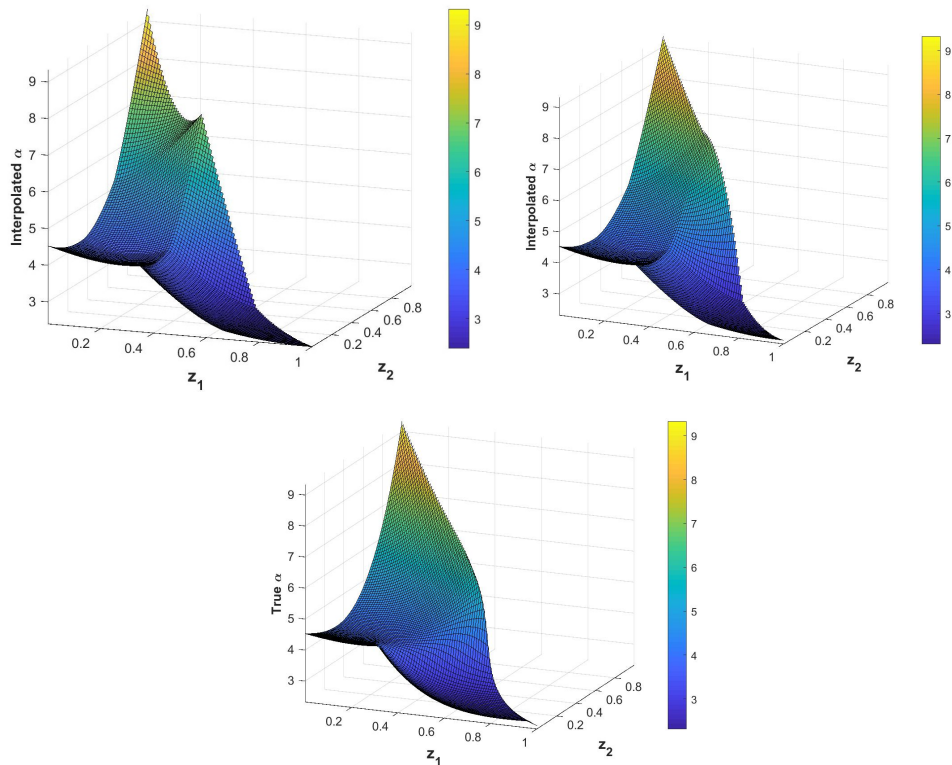


Figure 2.7: Euclidean accumulation operator α before extrapolation (top left), after extrapolation (top right) and true operator (bottom centre) at 56.6 bar with 4 resolution

In operator β , the maximum error is due to inconsistency in operator value, but after extrapolation the maximum errors in the plot corresponds to the nonlinearity in the operator.

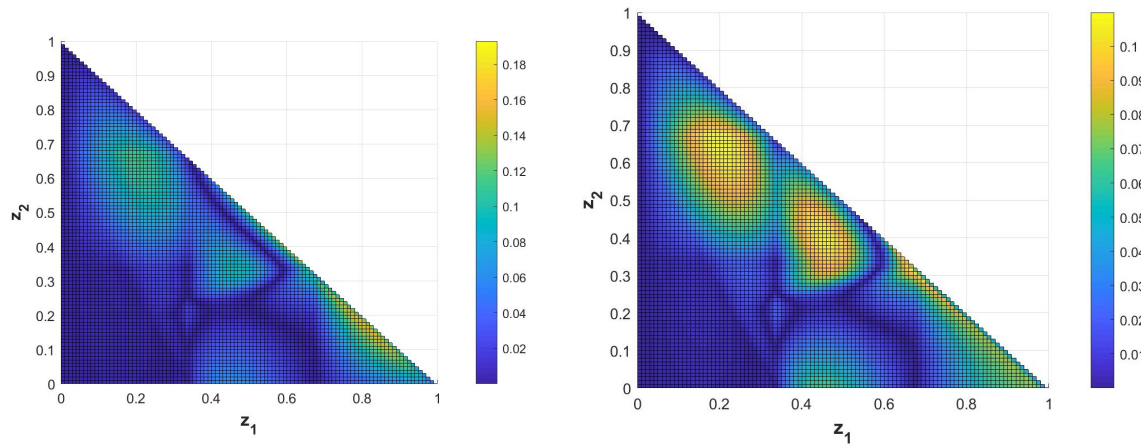


Figure 2.8: Number of Newton iterations for bi-linear and barycentric interpolation for Model 1(left) and Model 2(right)

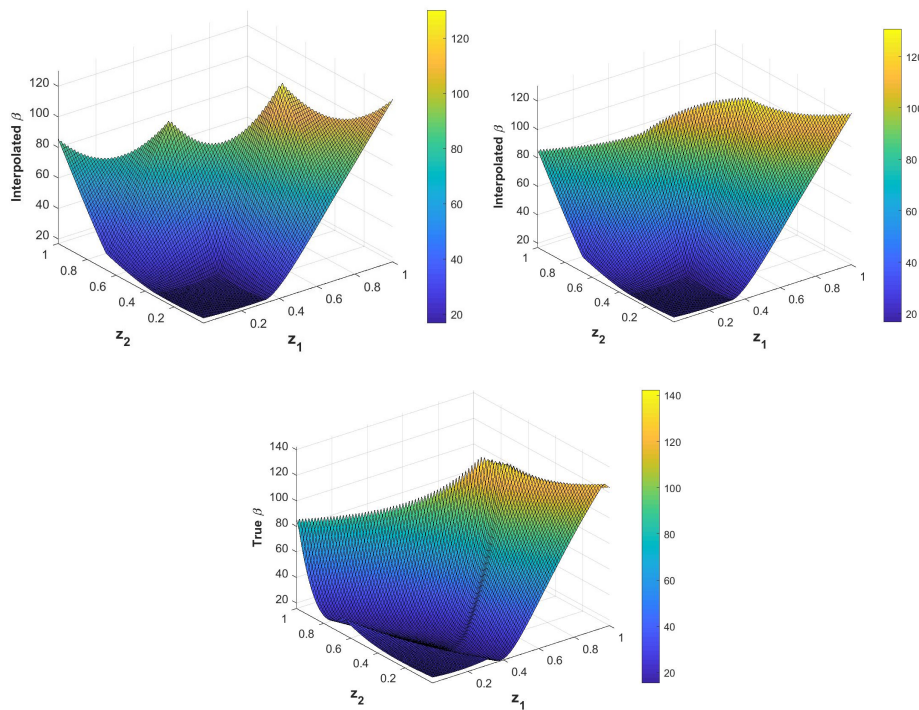


Figure 2.9: Euclidean accumulation operator β before extrapolation (top left), after extrapolation (top right) and true operator (bottom centre) at 56.6 bar with 4 resolution

The average errors before and after extrapolation strategy is presented in below table. A reduction of error is observed with with increase of resolution, as shown in the Table 2.2.

Table 2.2: Average error before and after extrapolation for EOS case

Operator	Resolution	Before Extrapolation	After Extrapolation
α	4	0.0231	0.0195
	16	3.89×10^{-3}	3.77×10^{-3}
	64	4.50×10^{-4}	3.42×10^{-4}
β	4	0.0468	0.0373
	16	7.17×10^{-3}	6.82×10^{-3}
	64	5.86×10^{-4}	4.20×10^{-4}

3

Interpolation Framework for Non-Uniform Mesh

The existing OBL framework employs piece-wise multi-linear interpolation, which is only applicable for uniform parameterization. In this chapter, we propose an alternative method of interpolation for dealing with arbitrary, non-uniform parameterization, represented with scattered data set of supporting points. It is performed in two steps:

1. the parameter space is tessellated into simplexes using Delaunay triangulation in an adaptive manner, based on scattered data set;
2. interpolation is performed within each simplex using barycentric coordinates of vertices with respect to the query point.

3.1. Delaunay triangulation

The Delaunay triangulation, introduced by (Delaunay et al., 1934) in 1934, is a method of triangulating the discrete set of points V into simplexes, a generalized notation of n dimensional triangle. For the triangulation, the set of simplexes formed from discrete points V should guarantee the empty circle property: circum-circle of each triangle surrounds only the vertices of that triangle but not any other point, as is shown in fig 3.1. This property makes the Delaunay triangulation unique in terms of mesh quality control, such as avoiding the presence of badly shaped simplexes with small angles, by maximizing the minimum angle of all simplexes.

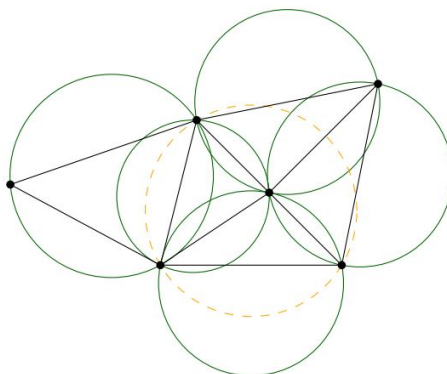


Figure 3.1: Triangles satisfying empty circle criterion

The boundary, within which Delaunay triangulation is performed, is called a *convex hull*. Constructing the convex hull ensures that tessellation is performed only in the physical do-

main of the problem. In this study, the convex hull corresponds to the physical domain of parameter space, which is shown by a red line in fig 3.2.

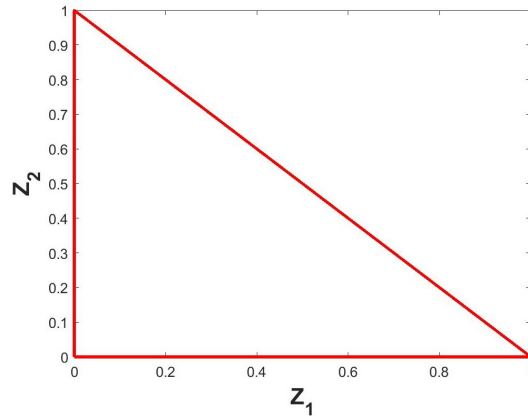


Figure 3.2: Convex hull representing the physical domain for triangulation space for three component system

3.1.1. Parameterization in Pressure and Composition

Parameterization in pressure and composition is performed differently: parameterization in pressure is performed in a uniform manner, while all other dimensions form subspace, where Delaunay triangulation is performed. Considering the parameter space for n_c components, the dimensions are $[p, z_1, \dots, z_{n_c-1}]$. The parameterization can be seen as $n_c - 1$ dimensional compositional subspaces are stacked together n times along the pressure axis $[p_1, p_i, \dots, p_n]$, where n represents the accuracy of uniform parameterization in pressure. The compositional subspaces are parameterized independently using Delaunay triangulation for each supporting point in pressure interval. The representation for three-component system is shown in fig 3.3.

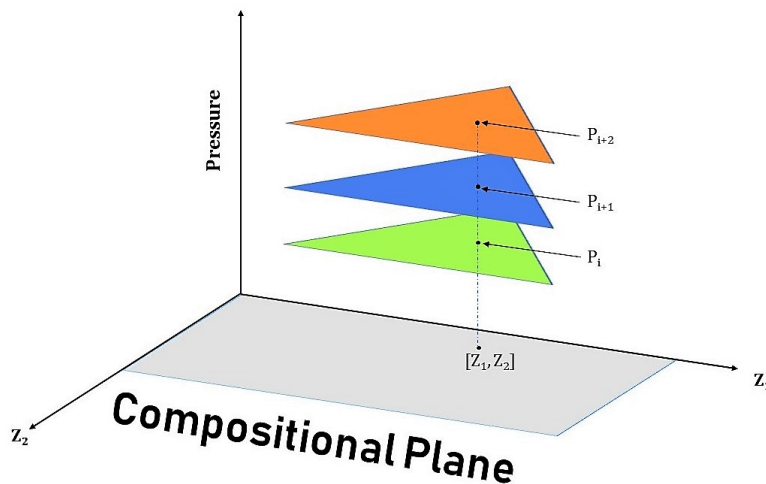


Figure 3.3: Representation of compositional planes along the pressure axis

3.2. Interpolation Framework

The combination of Delaunay tessellation and interpolation by finding barycentric coordinates is independent of shape/length of the geometric object (simplex) in the sub-domain. This facilitates for the treatment of a non-uniform mesh in physical parameter space. A detailed description on finding barycentric coordinates for 3-D and 4-D space is mentioned in Skala (2008). Barycentric interpolation for n dimensional convex hull is by Warren et al. (2007)

3.2.1. Estimating Operators

For a simplex of n_c vertices located at R_1, R_2, \dots, R_{n_c} , the weight of vertices γ_i corresponding to a query point R becomes barycentres of the vertices of simplex around R . Barycentric coordinates of each simplex are determined by solving the set of following linear equations where the sum of all the barycentric coordinates of simplex vertices is equated to 1:

$$\sum_{i=1}^{n_c} \gamma_i = 1. \quad (3.1)$$

For interpolating the query point R within the simplex, this can be written as a combination of the product of the barycentric coordinates and the corresponding vertices

$$R = \sum_{i=1}^{n_c} R_i \gamma_i, \quad (3.2)$$

where R represents the query point to be interpolated (within simplex), and R_i represents the vertices and γ_i indicates the barycentric coordinate corresponding to the vertex R_i .

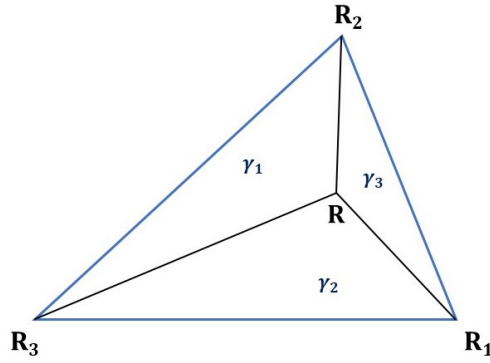


Figure 3.4: Schematic representation of a simplex with query point R and barycentres of each vertex

The system of linear equations 3.1 and 3.2 are expressed into a matrix form and can be linearly solved in barycentric coordinates:

$$\begin{bmatrix} \mathbf{R} \\ e \end{bmatrix} \Gamma = \begin{bmatrix} R \\ 1 \end{bmatrix}, \quad (3.3)$$

where R represents the query point to be interpolated, \mathbf{R} represents the coordinates of the simplex within which query point lies, e represents the unit vector arising from equation 3.1 and $\Gamma = \{\gamma_1, \gamma_2, \dots, \gamma_{n_c}\}$ denotes barycentric coordinates vertices around a query point in simplex of n dimensions.

3.2.2. Finding Derivatives

For studying compositional transport represented by governing equation 1.1, the derivatives of operators with respect to the nonlinear unknowns need to be computed. The derivatives of operators with respect to the composition of $n_c - 1$ components and pressure are described below.

Derivatives with Respect to Composition

Since barycentric coordinates linearly dependent on query point R , the derivatives with respect to composition will be constant within the simplex. Barycentric coordinates are dependent on the query points $[z_1 \text{ to } z_{n_c-1}]$. So, γ should be differentiated with respect to each

composition of the query point as shown below:

$$\frac{d\gamma_k}{dz} = \begin{bmatrix} \Gamma \\ e \end{bmatrix}^{-1} \hat{x}, \quad (3.4)$$

$$\frac{dR_i}{dz_j} = \sum_{k=1}^{n_c} R_k \frac{d\gamma_k}{dz_j}. \quad (3.5)$$

Here, $j = \{1, 2, \dots, n_c - 1\}$, $i = \{1, 2, \dots, n_c\}$, \hat{x} denotes the unit vector with unit value in j^{th} position, $\frac{dR_i}{dz_j}$ represents the derivative of operator w.r.t. to composition and $\frac{d\gamma_k}{dz_j}$ is the derivative of barycentric coordinate w.r.t. composition, which is now only dependent on the vertices of a simplex.

The derivative of operators resembles piece-wise linear constants within each simplex, making them discontinuous on the boundary of each simplex. To provide a smooth variation of derivatives, this method of computation needs more resolution to capture the continuity (smoothness) of the derivative.

Derivatives with Respect to Pressure

The derivatives of operators with respect to pressure are computed using linear interpolation of the operator values, obtained by barycentric interpolation in each of the two $n_c - 1$ dimensional compositional subspaces, build for pressures P_j and P_{j+1} . This is described below as

$$\frac{dR_i}{dP} = \frac{R_{P_{j+1}} - R_{P_j}}{P_{j+1} - P_j}, \quad (3.6)$$

where, dR_i/dP represents the derivative of operator about pressure at query point R for each component i .

3.2.3. Derivative Plots

Derivatives plots of operators α and β about $\{z_1, z_2\}$ computed from the newly proposed interpolation and multi-linear interpolation approaches are compared for three component $[CO_2, nC_4, C_{10}]$ fluid system at 60 bar pressure. The coarse uniform parameterization mesh is used for comparison.

A difference is observed in derivatives computed from multi-linear interpolation approach, and considerable variation is around the phase boundary. The derivatives within a simplex are constants as expected. The difference in derivatives between two approaches are shown in fig 3.7 and 3.8. It can be observed in error plots that the derivative from both the methods matches in the center of simplex, and the discrepancy is observed close to the edges. This difference is reduced with the addition of supporting points for a higher resolution.

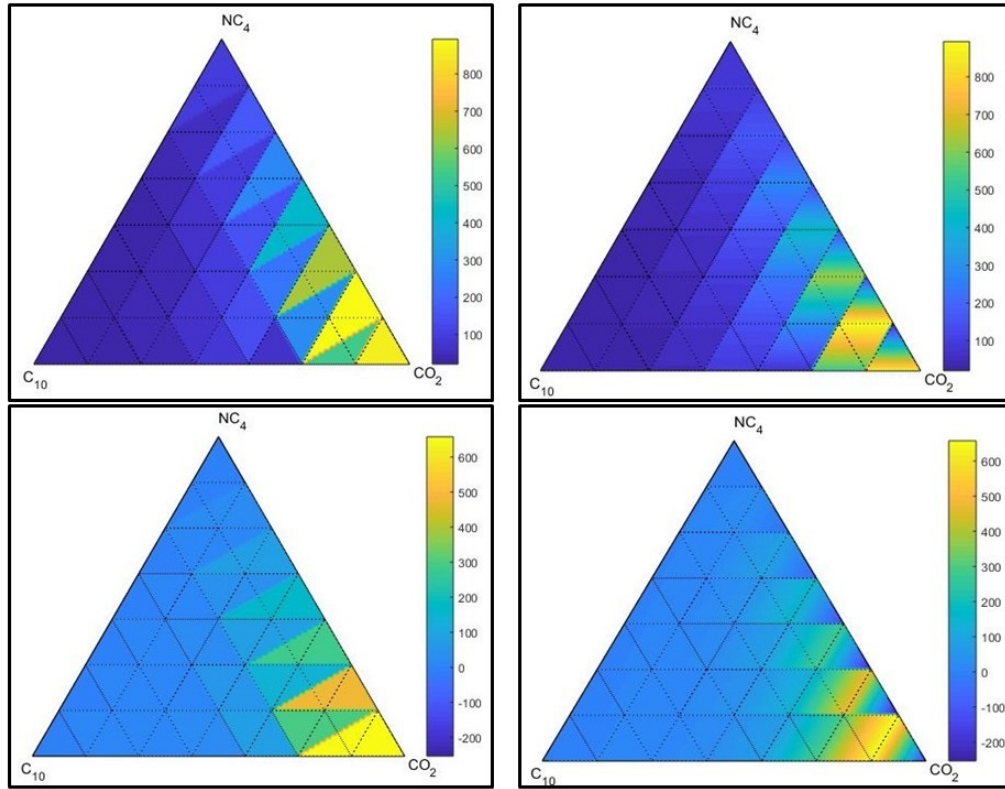


Figure 3.5: Derivatives of accumulation term about $\{z_1, z_2\}$ on top and bottom respectively, using barycentric interpolation (left) and multi-linear interpolation (right) at 60 bar

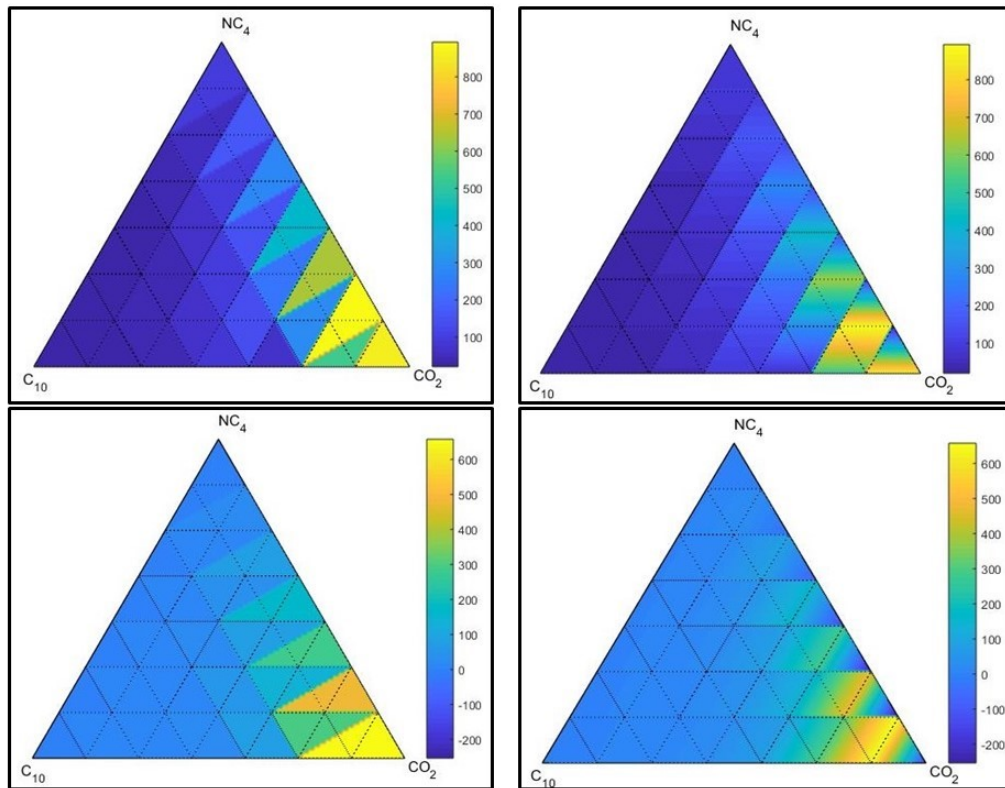


Figure 3.6: Derivatives of flux term about $\{z_1, z_2\}$ on top and bottom respectively, using barycentric interpolation (left) and multi-linear interpolation (right) at 60 bar

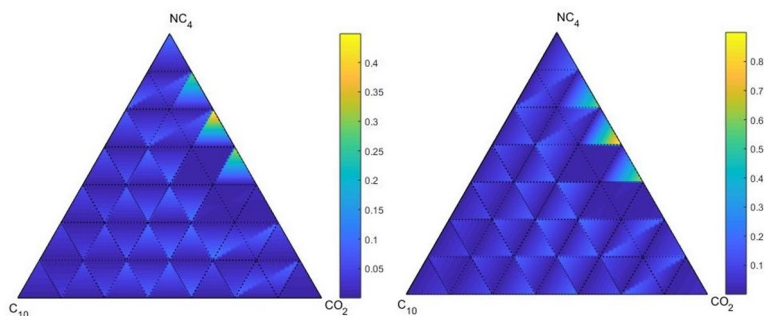


Figure 3.7: Error in derivatives of α to z_1 (left) and z_2 (right) with the two interpolation schemes at 60 bar pressure

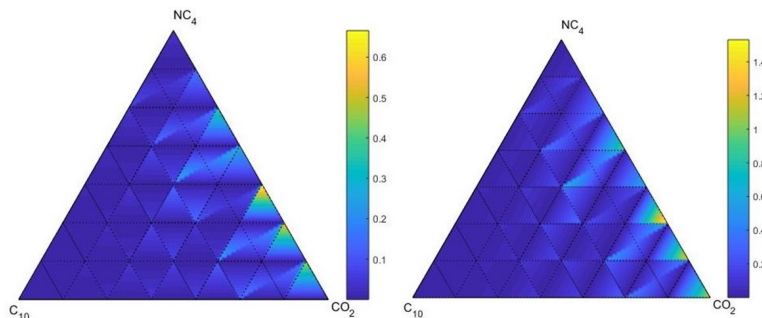
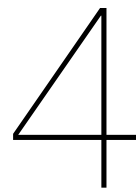


Figure 3.8: Error of derivatives β to z_1 (left) and z_2 (right) with the two interpolation schemes at 60 bar pressure

A higher error exists along the boundary $CO_2 - NC_4$ in the plots 3.7 and 3.8. This is because the multi-linear interpolation shares the supporting points from physical and non-physical space while performing interpolation close to physical boundary $z_1 - z_2$ in fig 3.2. This causes an inconsistent interpolation in operators which transcends into the derivatives, which is discussed earlier in Chapter 2

With an increase in resolution, the size of interpolation body decreases, so it accurately resolves the variation of operators in terms of its derivatives to unknown, which is observed in fig C.3 and C.4.



Adaptive Parameterization by Tie-Line Approach

OBL is a linearization technique which helps to simplify the problems associated with highly-nonlinear fully-coupled flow simulations. Since the existing OBL framework adopts multi-linear interpolation, the supporting points have to be uniformly distributed in parameter space, hence the parameterization does not honor the physics involved in governing eqn (1.1). The accuracy of the solution is influenced by the extent to which OBL can capture the nonlinearity involved. OBL constructs the operator approximations in a piece-wise linear manner, so at a lower resolution, it might not capture the nonlinear nature of the operator, thereby demanding higher density of supporting points.

In this study, we make use of two-phase tie-lines to accurately track the phase boundary and perform non-uniform parameterization. The motivation behind this adaptive construction is to reduce the maximum error in parameter space. This research idea is inspired from CSP approach by Voskov et al. (2007) and tessellating the compositional space into simplexes using tie-lines as demonstrated by Zaydullin et al. (2012), and Iranshahr et al. (2010). In this chapter, we adaptively parameterize the compositional space using tie-lines and demonstrate this parametrization for both constant K-values and EOS-based operators calculation.

4.1. Parameterization Scheme

Parameter set for molar formulation is $\{p, z_c\}$ and the variation of accumulation and flux operator is influenced by bubble point, dew point, and phase boundary. The phase behavior of a fluid system is represented in the bi-nodal curve, for a set of thermodynamic inputs of p bar and T^o K. For a given pressure, compositional space is a sub-domain of parameter space.

The line connecting liquid and vapor curve in phase envelope is called *tie - line*, along which phase compositions for liquid and vapor phases remains constant. The phase envelope is constructed as a set of tie-lines from the longest one to the critical point, where the length of tie-line becomes zero. So the tie-lines, which can follow the path of the phase boundary, is considered as a basis for parameterization.

The generalized idea of tie-simplex-based mathematical framework for an arbitrary number of phases was proposed by (Voskov and Tchepeli, 2009). The dimensionality of compositional space depends on the number of components and equals to $(n_c - 1)$. Since we are dealing with three component system the compositional space is a two-dimensional ternary diagram. Tie-line, corresponding to critical point, divides the compositional space into *subcritical* and *supercritical* space, as shown in Fig. 4.8. The adaptive parameterization approach is demonstrated for a non-isothermal compositional system of three components by (Khait et al., 2018a)

4.1.1. Constant K-values parameterization

As mentioned earlier, the critical point cannot be achieved for constant-K value. Since the attainment of the critical region is unimaginable, the parameterization is only restricted to the subcritical region in this case. The ternary representation of constant K is shown in fig 4.1 below. Two-phase region indicated by the liquid curve of $B_{ini} - B_1 - B_2 - B_3 - B_{inj}$ and vapor curve of $D_{ini} - D_1 - D_2 - D_3 - D_{inj}$.

The choice of injection and initial composition controls the extent of compositional space which should be parameterized. In order to cover the entire compositional space, z_{ini} and z_{inj} are taken along the vertices $Z_1 - Z_3$ and $Z_1 - Z_2$ of the ternary diagram 4.1. Initial and injection compositions are $[0.5-\epsilon, \epsilon, 0.5-\epsilon]$ and $[0.5-\epsilon, 0.5-\epsilon, \epsilon]$ respectively, where ϵ is of the order of 10^{-6} .

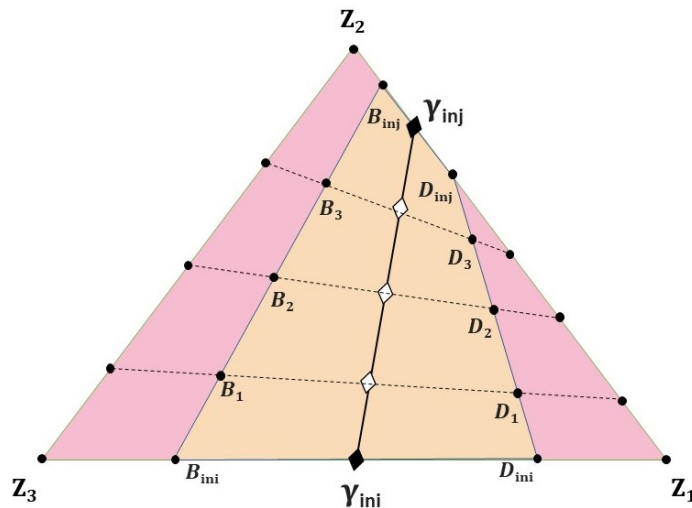


Figure 4.1: Ternary representation of parameterization scheme for constant K

For a given overall initial z_{ini} and injection compositions z_{inj} , liquid $x_{i,j}$ and vapor fractions $y_{i,j}$ are determined from two phase flash computations. Tie lines which connects between the between vapor and liquid fractions of z_{ini} , z_{inj} are drawn i.e. $D_{ini} - B_{ini}$ and $D_{inj} - B_{inj}$. For a well-behaved system hydrocarbon system, it can be assumed that tie-lines never intersect with each other inside the compositional space (Orr et al., 2007). Each tie-line can be uniquely represented by its midpoint γ in eqn. 4.1 (Entov et al., 2002).

The intermediate tie-lines between initial and injection tie-lines are determined by linearly interpolating γ_{ini} and γ_{inj} at a distance Δx between tie-line centers. Flash computations for all the set of intermediate γ help to trace the phase boundary between injection and initial compositions and parameterize the compositional space along two-phase boundaries.

In order to parameterize the single-phase region, ends of tie-lines are extrapolated. The tie-line which is extended on to the single-phase region is referred to as *parameterizing line*. Supporting points are added at the ends of the parameterizing line and on the phase boundary, complementing the physics involved. The parameterizing line is divided into segments by phase boundaries, and supporting points are added at a distance Δx in each segment.

$$\gamma = \frac{x_{i,j} + y_{i,j}}{2} \quad i = \{1, 2, \dots, n_c\}, \quad j = \{1, 2, \dots, n_p\} \quad (4.1)$$

4.1.2. EOS-based parameterization

EOS-based flash calculation brings a great deal of nonlinearity to the ternary diagram. The EOS-based calculations are responsible for the existence of closed phase boundary with a critical point separating the bubble and dew point curves. Now the entire compositional space is divided into the subcritical and supercritical region, which should be parameterized

separately.

The injection and initial compositions are taken from the previous section. The parameterizing lines are constructed for initial and injection composition from phase equilibrium computations, as mentioned above. Unlike in constant K value case, the compositional space is vertically parameterized along the midpoint of parameterizing lines, shown as $M_0-M_1-M_2-M_{cr}$ in fig 4.8. This minimizes the space (without parameterization) between tie-lines, as it goes from injection to initial composition. The problem aggregates when critical point shifts from the center of the phase envelope, giving rise to the dissimilar length of bubble and dew point curve. This might cause predominant interpolation error especially while modelling lean gas condensate reservoirs where critical point shifts towards the corner.

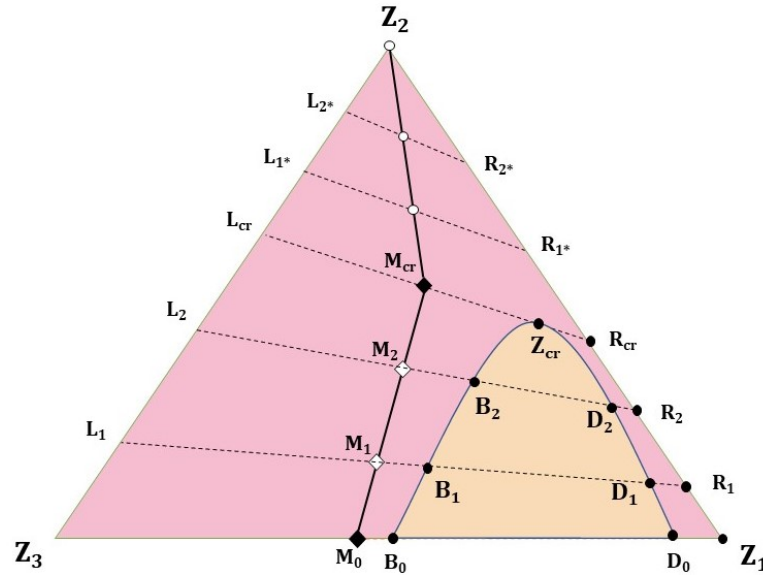


Figure 4.2: Ternary representation of parameterization scheme for EOS case

The entire procedure is demonstrated using the schematic representation in fig. 4.8. The two-phase region is indicated by the closure envelope B_0 to D_0 through Z_{cr} . Extension of critical tie-line on to edges of ternary diagram partitions the compositional space into the subcritical and supercritical region. Compositional space below and above $R_{cr}-M_{cr}-L_{cr}$ is classified as subcritical and supercritical region.

Representation of Subcritical Region

The number of tie-lines between the longest (B_0D_0) and critical tie-line is decided based on the midpoints of the parameterizing lines of z_{ini} and z_{inj} separated by the distance Δx .

$$N_{it} = \frac{|M_0M_{cr}|}{\Delta x} \quad (4.2)$$

Intermediate tie-lines are constructed by performing flash computations for a set of compositions between $M_0 - M_{cr}$, separated by Δx . Parameterizing line, which is an assembly of line segments $L_iB_i - B_iD_i - D_iR_i$, is developed. Finally, each line segment of single- and two-phase regions is parameterized by the distance Δx . This scheme is flexible enough to parameterize the single-phase and two-phase region with different Δx .

Representation of Super-critical Region

If the critical point does not exist for a given p bar and $T^\circ K$, then entire compositional space is parameterized as above. Here, the phase envelope shrinks with an increase in pressure,

giving rise to the supercritical region, as shown in fig 4.8. Length of the tie-line approaches zero at a critical point, making tie-lines irrelevant for parameterizing the super-critical space.

Supercritical region is parameterized along the line joining apex Z_2 and M_{cr} . Similar to the subcritical region, the number of lines $L_{i^*}R_{i^*}$ between $M_{cr}Z_2$ is determined as follows. The line segments $L_{cr}Z_2$ and $R_{cr}Z_2$ is equally divided into N_{il} , by distance Δx . Finally, each line segment $L_{i^*}R_{i^*}$ is partitioned by Δx ,

$$N_{il} = \frac{|M_{cr}Z_2|}{\Delta x}, \quad (4.3)$$

where $|M_{cr}Z_2|$ represents distance between Z_2 and M_{cr} .

4.2. Spatial Distribution of Errors

The supporting points in the adaptive mesh are scattered unevenly in compositional space. The tessellation is done by Delaunay triangulation, while interpolation is performed using barycentric coordinates. The effectiveness of adaptive construction in reducing error is analyzed by determining the spatial distribution of errors in compositional space at different pressures and comparing against uniform parameterization. The primary objective of adaptive construction is to reduce the maximum error in the parameter space rather than reducing the average error since the maximum error is caused by the virtue of underlying physics involved.

The quality of interpolation is defined by an absolute difference between true value and interpolated value at any point in parameter space. For simplicity, the Euclidean norm is used to combine the errors of n_c operators of each type i.e accumulation and flux operators. For unanimous representation, the error is normalized to the maximum value of the operator, which is mathematically described as

$$\|E_\alpha\|_j = \frac{\sqrt{\sum_{i=1}^{n_c} \left(\alpha_i^l(\omega_j) - \alpha_i^T(\omega_j) \right)^2}}{\max_{j,i} |\alpha_i^T(\omega_j)|}. \quad (4.4)$$

Here ω_j indicates the distribution of supporting points in compositional space, α_i^l and α_i^T represent interpolated and true operator value for a component i respectively.

For a fair comparison, nearly the same number of supporting points are taken between uniform and adaptive mesh. For a given Δx , the number of supporting points in uniform mesh remains constant throughout the pressure interval. For adaptive mesh, on the other hand, this number is susceptible to the size of phase boundary, thereby making it difficult to choose exactly the same number of points. So, acceptable range of $\pm 5\%$ of points is considered as an acceptable limit for comparison. Based on the adaptive mesh, the equal number of points in the uniform mesh is determined.

In a three component system at a given pressure, for uniform parameterization with n segments along each axis, there are in total n^2 supporting points. Out of which, $\frac{n(n+1)}{2}$ number of supporting points lie in physical space and $\frac{n(n-1)}{2}$ belonging to non-physical space. The number of physical points in both cases is equated to know the discretization intervals for getting a similar number of supporting points in the uniform mesh

$$\frac{n(n+1)}{2} = N_{adaptive}, \quad (4.5)$$

where $N_{adaptive}$ indicates the number of supporting points in adaptive mesh.

4.3. Results

We adaptively parameterize the ternary representation of three component fluid system [CO_2 , nC_4 , C_{10}] at three different pressures and a fixed temperature of $345^\circ K$.

4.3.1. Constant K-values parametrization

The ternary representation at 75 bar pressure is shown in fig 4.3. High nonlinearity is observed in flux operator β , which is due to nonlinearity induced by density and Brooks-Corey relation in calculating of relative permeability. The two-phase region is not clearly observed in accumulation operators, but to a certain extent, the phase boundary is identified in flux term by observing the variation of the operator in fig. 4.6.

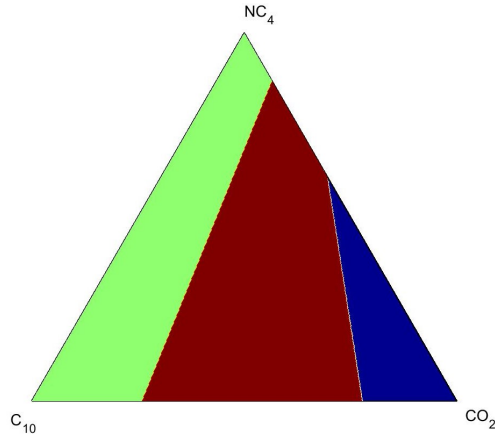


Figure 4.3: Ternary representation of phase diagram for constant K values at 75 bar and $345^\circ K$

The compositional space is finely discretized into small intervals, referring each point as a *query point* and the operators are interpolated using the supporting points in the adaptively constructed mesh. The normalized interpolation error of operators are plotted for uniform and adaptive parameterization in fig 4.5, 4.7. Adaptive construction generates 42 supporting points and the corresponding closest number of supporting points in the uniform mesh is 45. It is observed that adaptive mesh resolves the nonlinearity around phase interface better than uniform mesh even with a slightly lower number of supporting points, which is reflected in the reduction of maximum error.

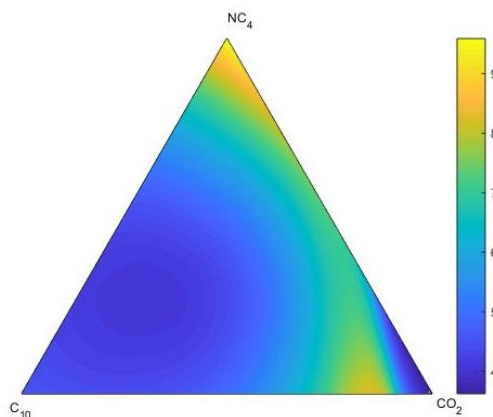


Figure 4.4: Euclidean operator plots of accumulation term α at 75 bar and $345^\circ K$

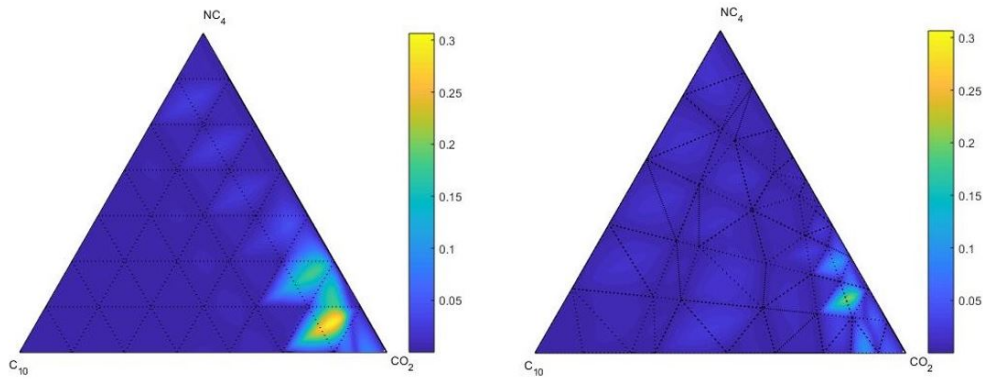


Figure 4.5: Euclidean error in accumulation operator at 75 bar for uniform mesh (left) adaptive(right) with 45 and 42 supporting points respectively

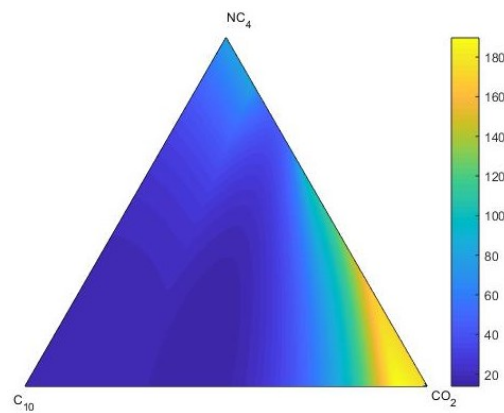


Figure 4.6: Euclidean operator plots of accumulation term β at 75 bar and 345° K

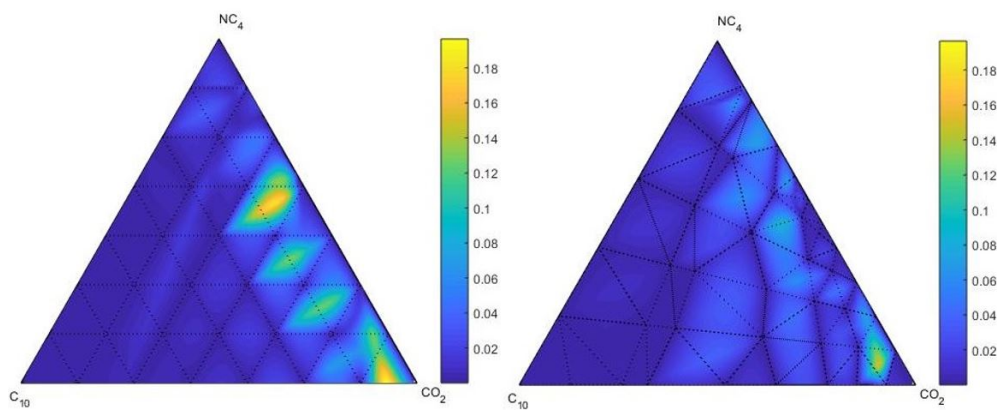


Figure 4.7: Euclidean error in flux operator at 75 bar for uniform (left) adaptive(right) mesh with 45 and 42 supporting points respectively

4.3.2. EOS-based parametrization

The ternary representation of the fluid system at three different pressures 30, 65 and 100 bar is shown in fig 4.8. It can be seen that the two-phase region is sensitive to pressure and shrinks with the increase in pressure. At higher pressures above 100 bar, the two-phase region within compositional space is relatively small so we considered 100 as the upper

pressure limit. At 30 and 65 bar pressures, subcritical parameterization can parameterize the entire compositional space, but at higher pressures when the fluid has critical point at the combination of p and T , super-critical representation is needed.

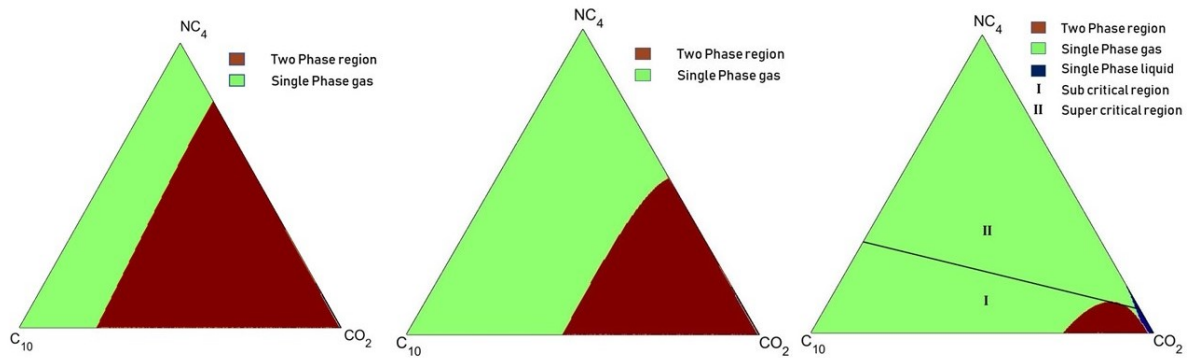


Figure 4.8: Ternary representation of phase diagrams at pressures 30, 65, 100 bar at 345° K for fully EOS case

The Euclidean norm of operators α and β are shown in fig. 4.9 and fig. 4.12. Unlike constant K , there exists a strong coupling between thermodynamic behavior and composition. This can be seen in operator plots, which accurately captures the phase interface i.e. boundary separating single and two-phase region. A clear contrast can be seen along the boundary, this can be due to nonlinearity associated with endpoint relative permeability effect.

Adaptive parameterization accurately captures the two-phase region using tie-lines, as shown in the figures 4.10 and 4.13. Here, the number of supporting points is susceptible to the sub-critical and supercritical region and it is difficult to control compared to uniform mesh. The number of adaptive and uniform points at three pressures are shown in Table 4.1.

Table 4.1: Number of supporting points in uniform and adaptive mesh for EOS case

p (bar)	$N_{Uniform}$	$N_{Adaptive}$
30	45	44
65	45	47
100	78	76

As observed in fig. 4.10 and fig. 4.14, the maximum errors are concentrated along the two-phase interface due to the drastic change in operator and inability of interpolation to follow the nonlinearity. Using tie-lines, the two-phase boundary is complemented with supporting points. However, the region close to the critical point is highly nonlinear, an additional tie-lines are added between the final and penultimate tie-line to handle this region.

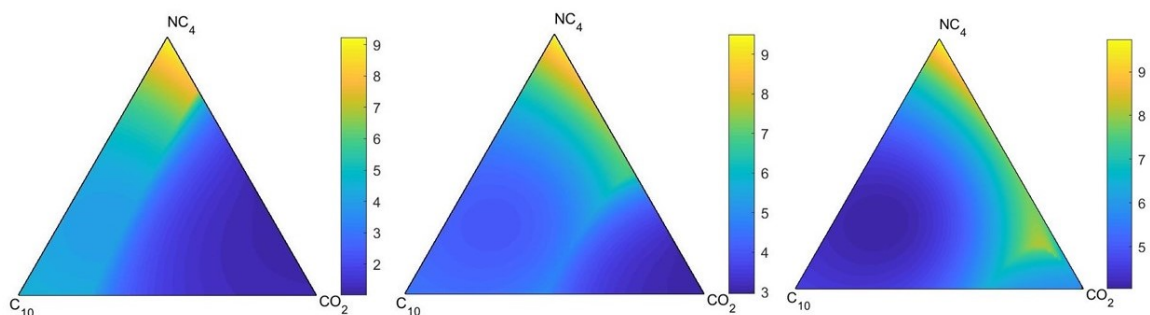


Figure 4.9: Euclidean operator plots of accumulation term α at 30, 65, 100 bar and 345° K

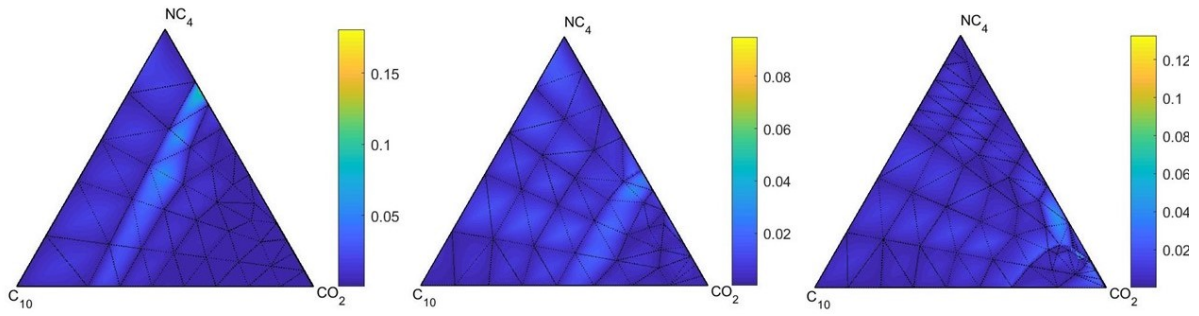


Figure 4.10: Error in accumulation operator using adaptive parameterization at 30, 65, 100 bar for composition CO_2 , NC_4 , C_{10}

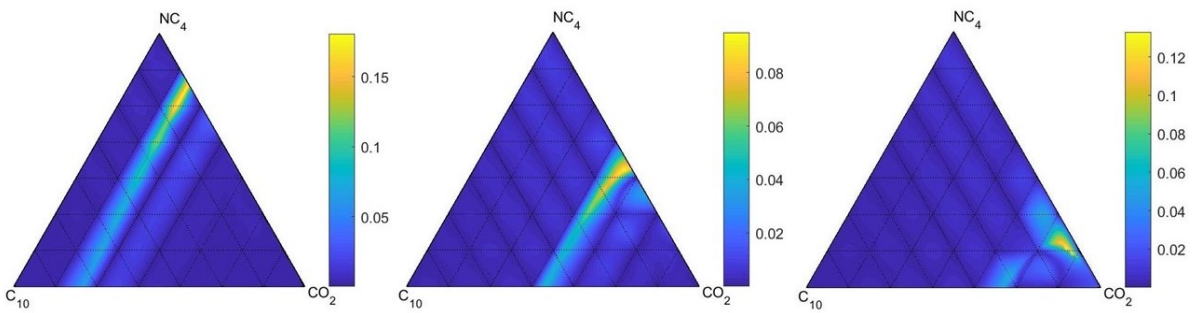


Figure 4.11: Error in accumulation operator using uniform parameterization at 30, 65, 100 bar for composition CO_2 , NC_4 , C_{10}

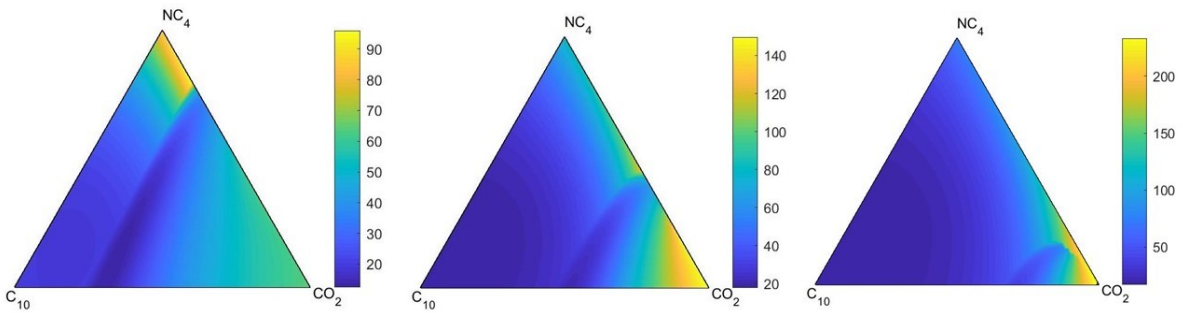


Figure 4.12: Euclidean operator plots of flux term β at 30, 65, 100 bar and $345^\circ K$

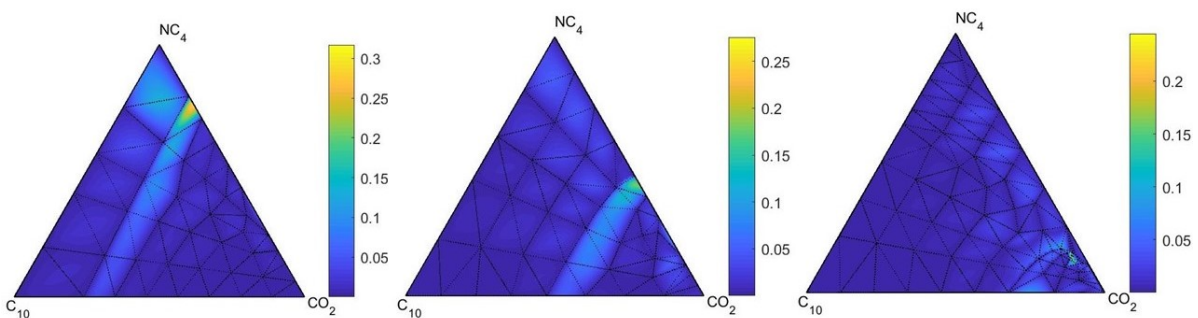


Figure 4.13: Error in flux operator using adaptive parameterization at 30, 65, 100 bar for composition CO_2 , NC_4 , C_{10}

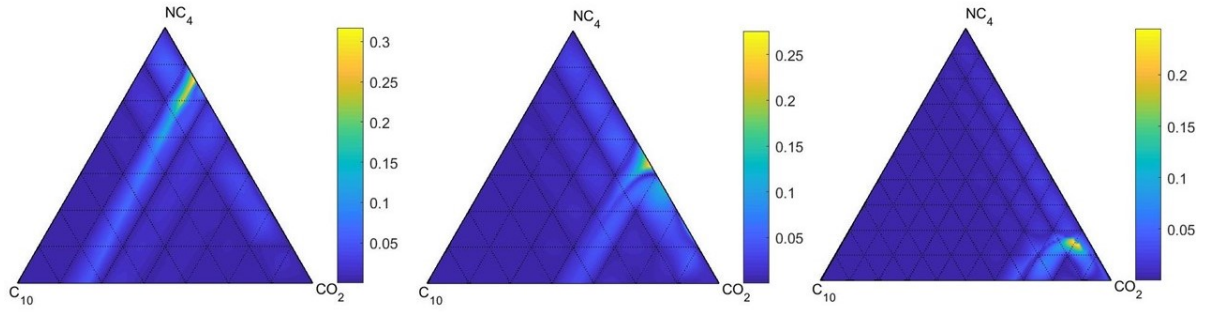


Figure 4.14: Error in flux operator using uniform parameterization at 30, 65, 100 bar for composition CO_2 , NC_4 , C_{10}

4.3.3. Sensitivity Analysis

The maximum error in the compositional space is considered for performing sensitivity analysis. Variation of maximum error and the number of supporting points are plotted on semi-log plot on the x-axis for five intervals between Δx 0.1 and 0.01.

Constant K-values parametrization

The sensitivity analysis for this case is performed at three different pressures of 30, 75 and 120 bars. The effectiveness of adaptive mesh can be seen in fig. 4.15 and fig. 4.16. An irregular behavior of error is observed at lower pressure. This happened due to the fixed geometric constraint associated with Delaunay triangulation. Due to the larger distance between the ends of tie-lines shown in fig. C.2, the triangles become pointy, causing large interpolation errors. This geometric constraint usually disappears with an increase in pressure.

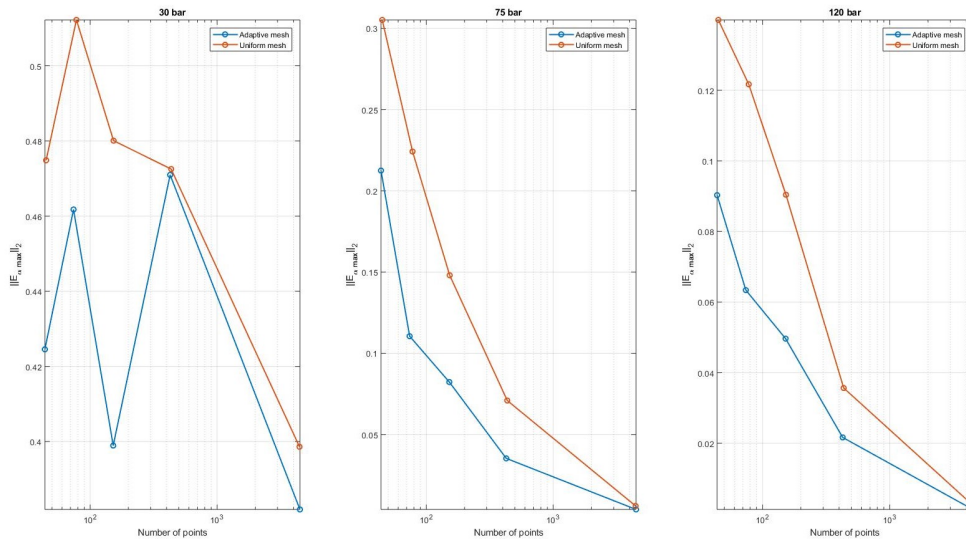


Figure 4.15: Variation of maximum error in accumulation term for uniform and adaptive mesh at 30, 75, 120 bar respectively

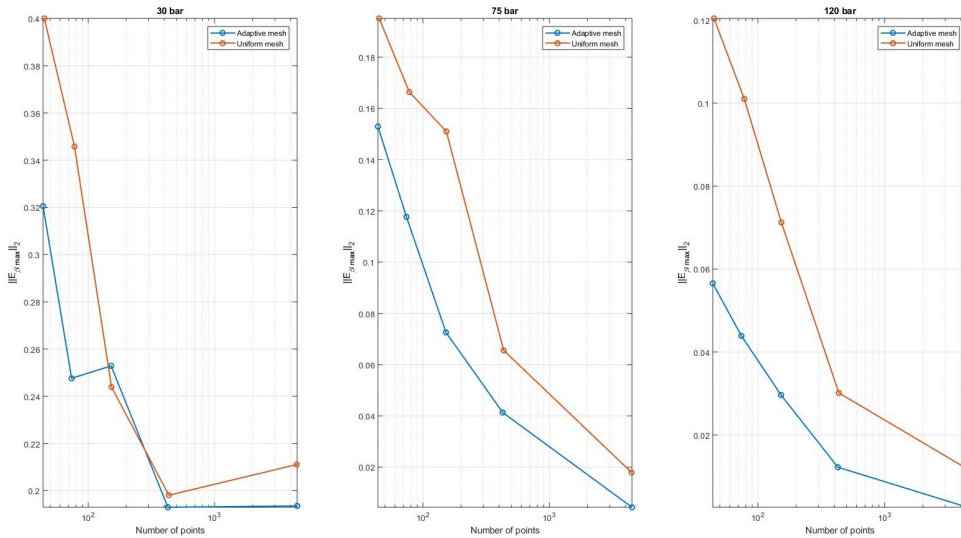


Figure 4.16: Variation of maximum error in flux term for uniform and adaptive mesh, at 30, 75, 120 bar respectively

EOS-based parametrization

With high resolutions at small Δx , the supporting points are densely populated in parameter space. The uniform mesh can resolve the nonlinearity of operator, thereby reducing the difference in maximum error between uniform and adaptive mesh. At times uniform mesh gets lucky enough to find few of its supporting points exactly on the nonlinear region, making it better than adaptive mesh. This is observed in sensitivity plot of α and β at 30 bar in fig 4.17 and 4.16.

A non-monotonic trend is observed with sensitivity plots 100 bar in α and β . A high nonlinearity is observed close to the critical region in operator plots at 100 bar, making the error highly sensitive to small perturbations of distance δx . However, still, the adaptive construction performs better than uniform mesh. Non-monotonic change in error of flux term is due to the highly nonlinear variation of the two-phase interphase close to the critical region. But adaptive mesh manages to keep lower maximum error.

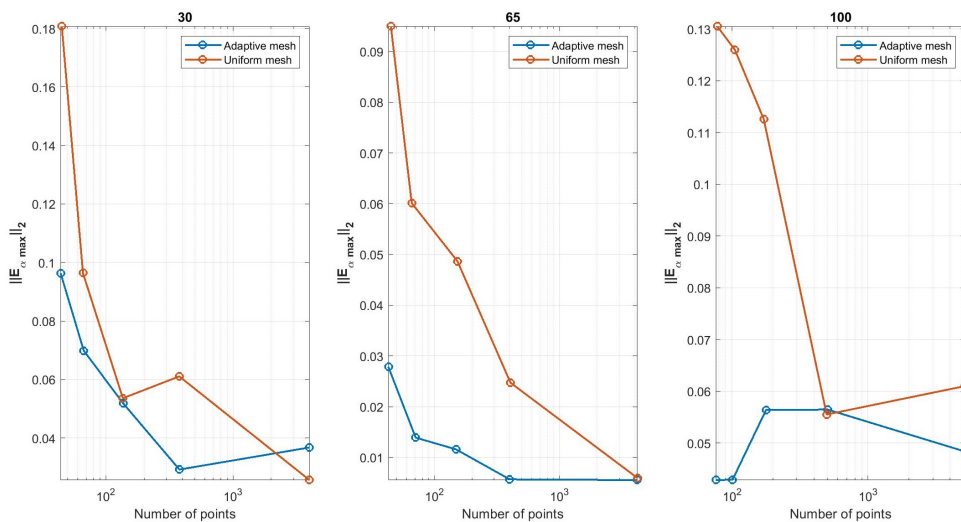


Figure 4.17: Variation of maximum error with refinement in accumulation operator α for uniform and adaptive mesh at 30, 75, 120 bar respectively

At 65 bar, the difference in error between uniform and adaptive mesh decreases with

higher resolution, which is a normally expected trend, because both get closer to the reference solution.

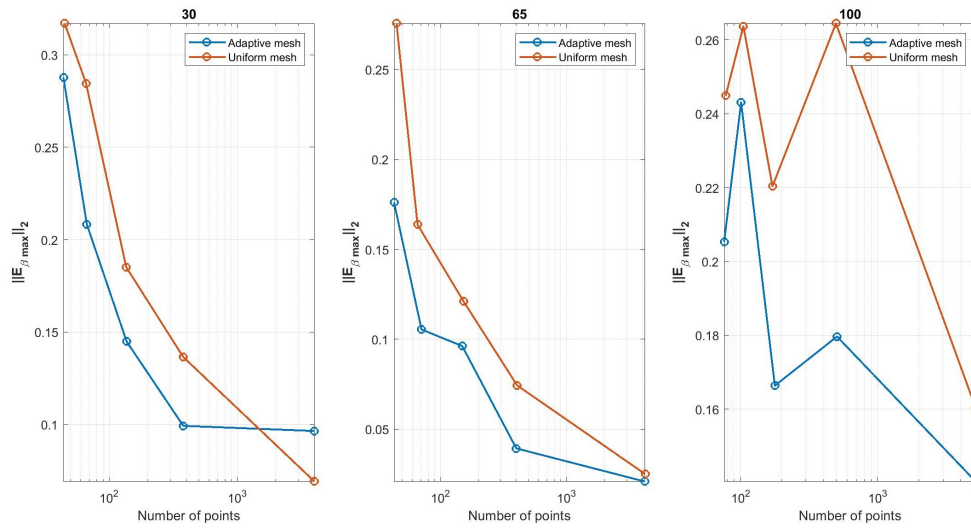


Figure 4.18: Variation of maximum error with refinement in flux operator α for uniform and adaptive mesh, at 30, 75, 120 bar respectively

5

Validation of Tie-Simplex Parameterization

In this chapter, the newly proposed tie-simplex framework is validated for one-dimensional simulation of the governing transport equation (1.1) for three component system. The accuracy of tie-simplex parameterization is compared with uniform parameterization and nonlinear Newton convergence study is carried out by comparing the two methods. Extension of the framework to the multicomponent system is discussed by considering a four component fluid system.

5.1. Transport Solver

The practical applicability of tie-simplex parameterization is assessed by testing it with a robust, fully implicit one-dimensional transport solver. This 1D solver represents a homogeneous reservoir model which studies the interaction of different components locally and transport of these individual species over the length of the reservoir. The reservoir is discretized into grid blocks and constant Bottom Hole Pressure (BHP) controls at 100 bar and 60 bar are applied at injector and producer, which are present in the first and last grid block respectively. The fluxes between grid blocks are caused by the pressure difference. For the simplicity of the solution, capillary and gravity effects are neglected, making the pressure potential solely responsible for the transport of components. We model the production of intermediate nC_4 and heavier C_{10} hydrocarbons by injecting of CO_2 at the injector.

5.1.1. Scheme of Solver

As mentioned earlier, nonlinear Newton's solver is used to solve the linear system of equation 1.15. The convergence of this nonlinear solver is based on the following criterion:

$$\|r\|_2 < 10^{-4},$$

where r is a residual vector of length equal to number of grid blocks.

A constant multiplication factor t_{mult} is used in timestepping criterion. If the nonlinear solver converges for the current timestep (Δt_i), next timestep is defined as $\Delta t_{i+1} = \Delta t_i * t_{mult}$, until the maximum size of the timestep (Δt_{max}) is reached; if the nonlinear solver fails to converge, then we repeat the attempt with new timestep $\Delta t_{i+1} = \Delta t_i / t_{mult}$. If the nonlinear solver consecutively fails to converge and when the timestep reaches below minimum tolerance value, the simulation is aborted. Physical properties of this homogeneous reservoir model and input parameters used in the simulation are mentioned in *Appendix 2*.

The Jacobian system is solved at every nonlinear iteration. The nonlinear update is applied to the set of unknown variables (p, z_1, z_2). Since the governing equation is hyperbolic in nature, there is a high chance for solution exceeding the physical bounds, the composition

in particular. So, before updating the solution, the following correction check is performed at the end of every successful Newton convergence to ensure the solution is in physical bounds:

- The first stage is a local chopping of the update, such that the absolute value of the update is smaller than a predefined value of 0.1;
- All the compositions are corrected such that their values remain in the physical range of [0 to 1].

5.2. Validation

The lower and upper bounds of pressure and composition constitute parameter space i.e. $[20, 130]$ bar $\times [0, 1]^{n_c-1}$. We run simulations with OBL framework using barycentric and multi-linear interpolation at different resolutions.

Transport equation is time-dependent hyperbolic, the shocks and rarefaction are observed in the displacement profile. The solution at time when the leading shock reaches the producer is shown in 5.1. Two simulation models were considered: one with 100 (Model 1) and more refined model with 500 grid blocks (Model 2). For different resolution, the displacement profiles at the end of simulation using barycentric interpolation for uniform mesh are shown below. It is evident that the shape of the solution is accurately captured at resolution with 16 points only.

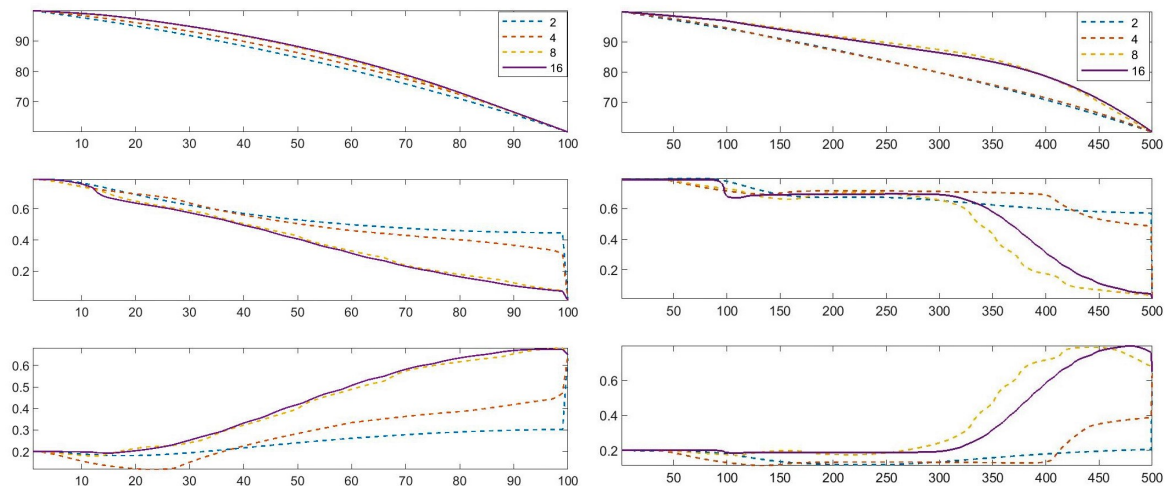


Figure 5.1: Displacement profile of 1D simulation for Model 1 on left and Model 2 on right at resolutions 2,4,8,16 for uniform mesh using barycentric interpolation

5.3. Accuracy of Solution

The accuracy of tie-simplex parameterization is compared with multi-linear interpolation. The spatial error induced by the interpolation is determined by the Euclidean norm of difference averaged over each grid block. The normalized average errors in pressure and composition are plotted for three different resolutions. The error induced in each grid block depends on the size of the interpolation body and proximity between the supporting points and the solution path followed by each grid block over the course of the simulation. The error is accumulated in every Newton's iteration for all the timesteps. With a finer resolution, supporting points are densely populated in parameter space, thereby increasing the closeness between the solution path followed and supporting points, which in turn increases the accuracy and exactness of interpolation.

$$\|E_Y\| = \frac{\sqrt{\sum_{i=1}^{NB} (Y_i^I - Y_i^T)^2}}{\max |Y^T| * NB}, \quad Y = [p, z_1, z_2, \dots, z_{nc-1}] \quad (5.1)$$

Where, NB indicates the number of grid blocks, I , T represents multi-linear and barycentric interpolation respectively and $\max(Y^T)$ indicates the maximum of unknowns computed with multi-linear interpolation during simulation. This depends on initial and injection parameters.

5.4. Nonlinear Convergence Study

This study provides a conclusive evidence on the effectiveness of the tie-simplex method in handling the nonlinear Newton's iterations and its rate of convergence. We refer the iterations of current timestep in which the nonlinear solver fails to meet residual tolerance as *wasted iterations*. For a fair comparison, the smallest timestep is considered to which all the three resolutions we considered converge with no wasted iterations. Lower the initial timestep, better will be the convergence during the start of the simulation. A maximum timestep (Δt_{max}) of 0.2 days is taken for three component system and 0.9 days for 4 component system.

5.5. Results

Error between unknowns at the end of simulation is plotted on a semi-log plot of error on y-axis and resolution on the x-axis. Error plots are shown with absolute error to its maximum of each unknown. Newton's iterations are presented on bar graph on the y-axis, the resolution on the x-axis.

5.5.1. Three Component System

Three component fluid system of $[CO_2, nC_4, C_{10}]$ is considered with initial and injection conditions as

Table 5.1: Injection and production conditions for 3 component fluid system

	p (bar)	CO_2	nC_4	C_{10}
Injection	100	0.79	0.2	0.01
Production	60	0.01	0.65	0.34

Constant K-values parameterization

The solution from multi-linear interpolation is taken as reference. It can be seen in fig. 5.3 that the first simulation model with 100 blocks has less error compared to model 2 consisting 500 blocks and the error is decreasing logarithmically with resolution. Errors are mainly due to slight changes in the shape of rarefaction part and around the shock front of the solution, as seen in fig. 5.2.

Table 5.2: Error of unknowns in tie-simplex parameterization in comparison with multi-linear interpolation for constant-K

Model	Resolution	$Error_p$	$Error_{z_1}$	$Error_{z_2}$
Model 1	16	3.96×10^{-5}	3.69×10^{-4}	2.31×10^{-4}
	64	8×10^{-6}	1.37×10^{-4}	6.54×10^{-4}
	128	2.34×10^{-6}	5.15×10^{-5}	4.15×10^{-5}
Model 2	16	6.57×10^{-5}	8.26×10^{-4}	9.63×10^{-4}
	64	1.29×10^{-5}	1.75×10^{-4}	1.26×10^{-4}
	128	4.41×10^{-6}	7.72×10^{-5}	6.87×10^{-5}

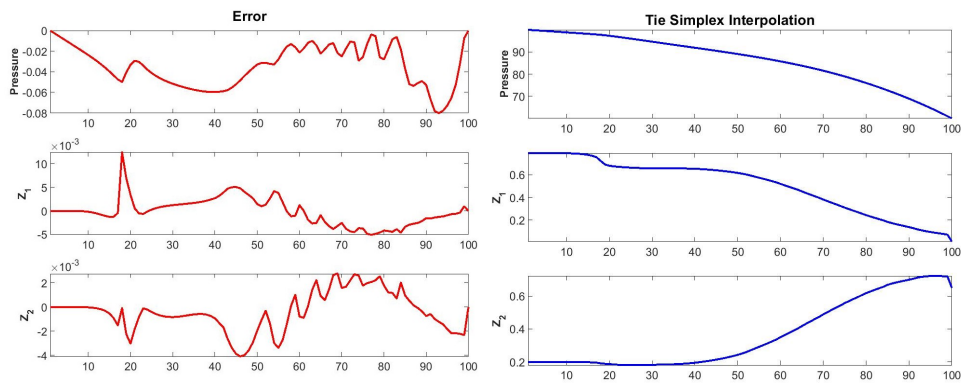


Figure 5.2: Error of unknowns at every grid block in the reservoir model 1 (on left) and solution from tie-simplex parameterization (on right) for resolution 16

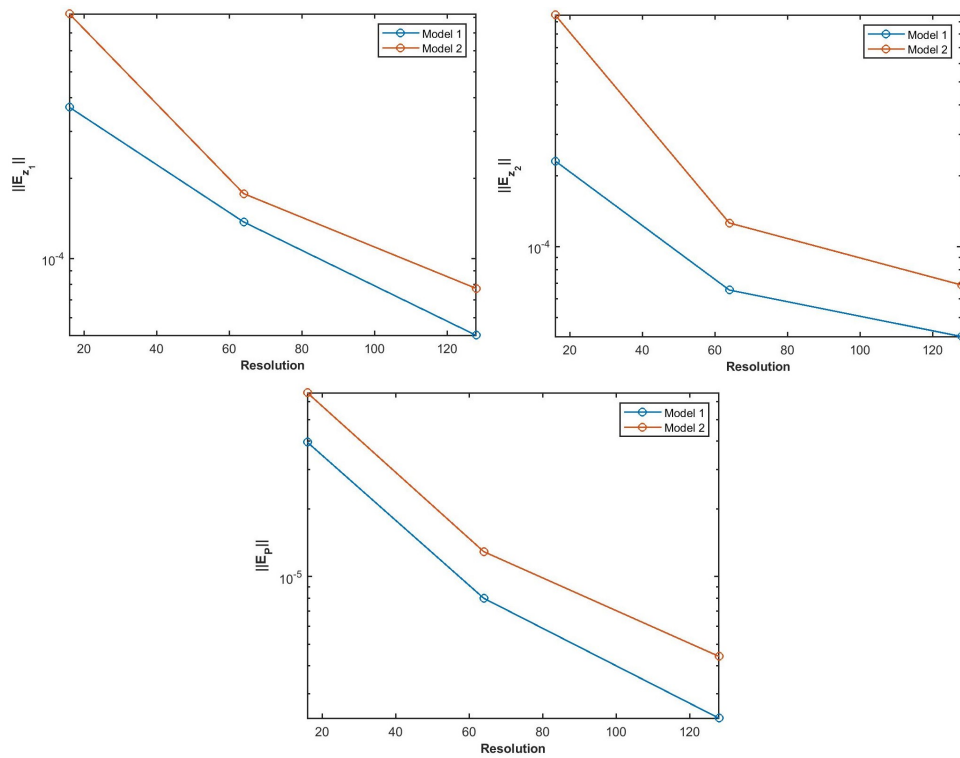


Figure 5.3: Average error in pressure and composition for each grid block for longer and shorter models at resolution 16, 64, 128

As discussed earlier, the Jacobian assembly with respect to nonlinear unknowns influences the rate of convergence. In tie-simplex case, the derivatives are constant inside the simplex where it changes slightly within hypercube of the multi-linear interpolation. This can be observed in fig 3.5, and 3.6. But with an increase in resolution, the size of simplex reduces and a smooth trend in variation of derivatives is observed, thereby reducing the difference in derivatives between the two interpolation schemes as can be seen in fig. C.3 and fig. C.4.

This theory implies that difference in the number of Newton’s iterations between these two interpolation schemes is expected to decrease with an increase in resolution, which can be observed in the fig. 5.4. Sometimes, the above-mentioned theory cannot be established with shorter models because of the behavior of Newton’s solver, the rate of convergence and the due to convergence criterion taken. So it is advisable to consider the longer models.

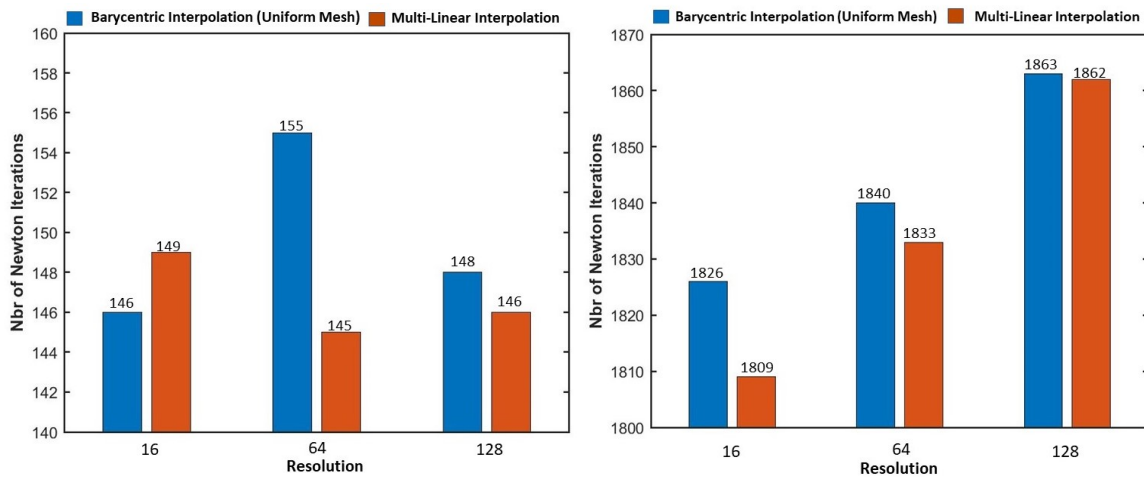


Figure 5.4: Number of Newton’s iterations of barycentric interpolation and multi-linear interpolation with uniform mesh for Model 1 (on left) and Model 2 (on right) for three component system with constant K values

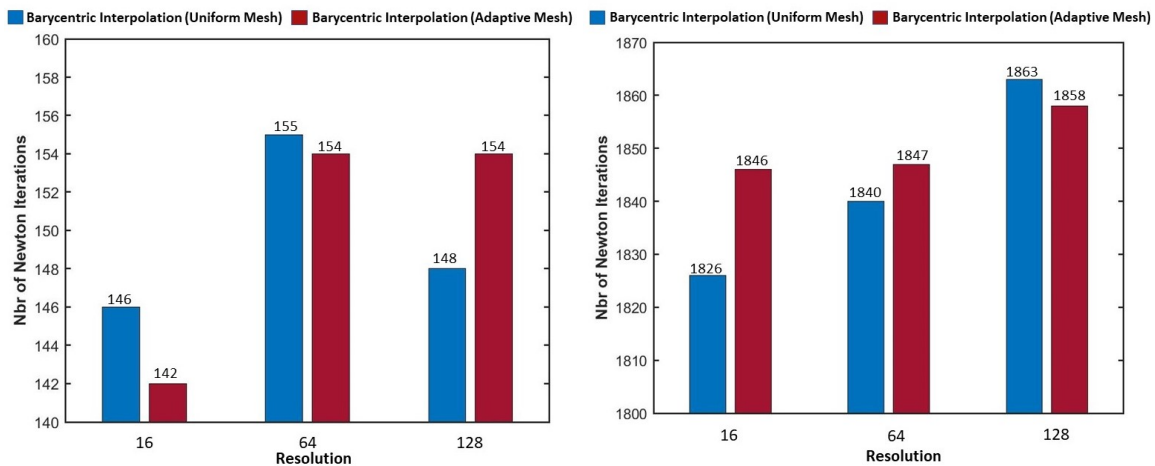


Figure 5.5: Number of Newton’s iterations of barycentric interpolation with uniform mesh and adaptive mesh for Model 1 (on left) and Model 2 (on right) for three component system with constant K values

It’s challenging to consider an equal number of supporting points in adaptive mesh compared to uniform mesh, the closest number of supporting points is taken. The average number of supporting points for all the pressures in parameter space is given below, but the number varies with each pressure in the adaptive mesh.

Table 5.3: Average number of supporting points for uniform and adaptive mesh for constant K values

Resolution	Uniform Mesh	Adaptive Mesh
16	136	132
64	2080	2064
128	8256	8252

In general, adaptive mesh consumes more iterations compared to uniform mesh. This is attributed to the variation in the size of a simplex in parameter space. During simulation with the adaptive mesh, the solution can change through several simplexes with very different size. Since the nonlinearity around the phase boundary is captured, it gives better accuracy than uniform mesh. However, it can be seen from fig 5.5 that the difference in Newton iterations are less between uniform and the adaptive mesh.

EOS-based parameterization

Similar trend in error is observed for Fully EOS.

Table 5.4: Error of unknowns in tie-simplex parameterization in comparison with multi-linear interpolation for fully EOS case

Model	Resolution	$Error_p$	$Error_{z_1}$	$Error_{z_2}$
Model 1	16	1.07×10^{-4}	4.86×10^{-4}	3.94×10^{-4}
	64	6.45×10^{-5}	1.42×10^{-4}	4.29×10^{-5}
	128	7.32×10^{-6}	4.85×10^{-5}	2.14×10^{-5}
Model 2	16	6.57×10^{-4}	8.26×10^{-4}	9.63×10^{-4}
	64	1.29×10^{-5}	1.75×10^{-4}	1.26×10^{-4}
	128	4.41×10^{-6}	7.72×10^{-5}	6.87×10^{-5}

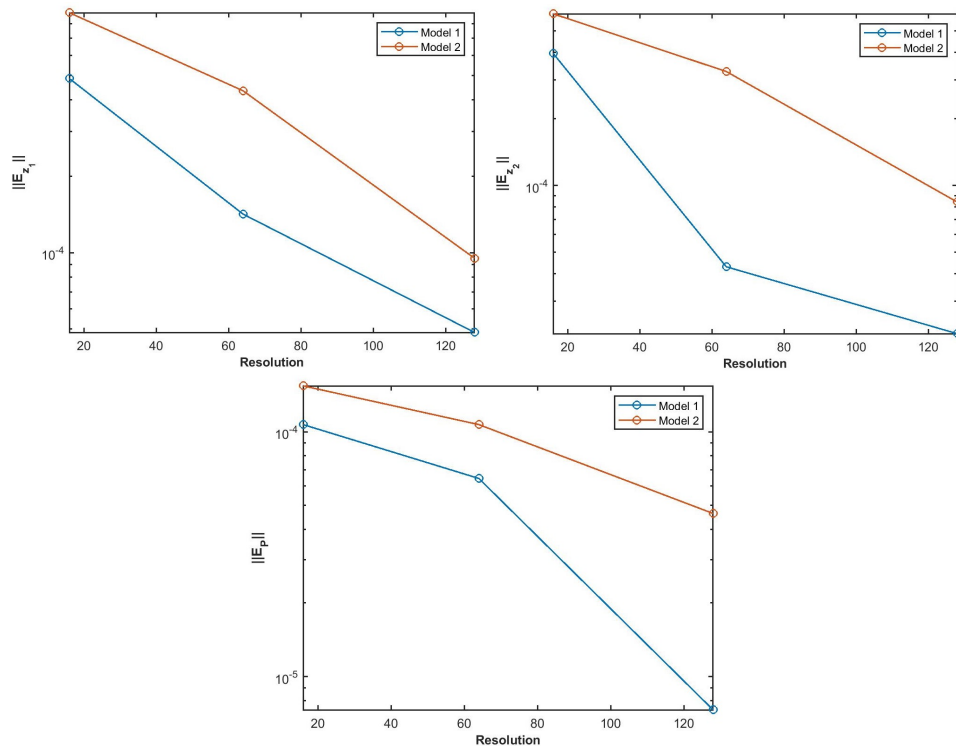


Figure 5.6: Average error in pressure and composition for each grid block for longer and shorter models at resolution 16,64,128 for three component fully EOS case

The difference in Newton's iterations is increasing with resolution in the first model. This is because nonlinear solver converges with great difficulty with multi-linear interpolation. In order to confirm this, the same model is run for a different maximum timestep of (Δt_{max}) of 1 day, where a normal trend is observed as shown in fig. 5.8. This confirms that tie-simplex approach shows better convergence rate for Newton's solver whereas multi-linear case struggles at different timesteps. Since the derivative is constant within simplex, the unique derivative values in the Jacobian assembly are less when constructed with the tie-simplex approach, which helps "nonlinear solver to converge faster".

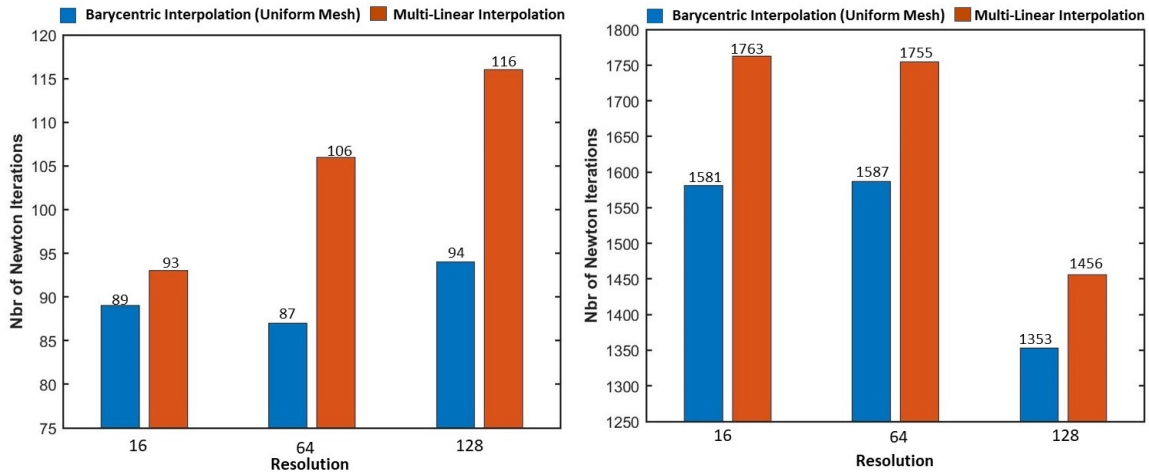


Figure 5.7: Number of Newton's iterations for barycentric and multi-linear interpolation for Model 1 (left) and Model 2 (right) for three component fully EOS case

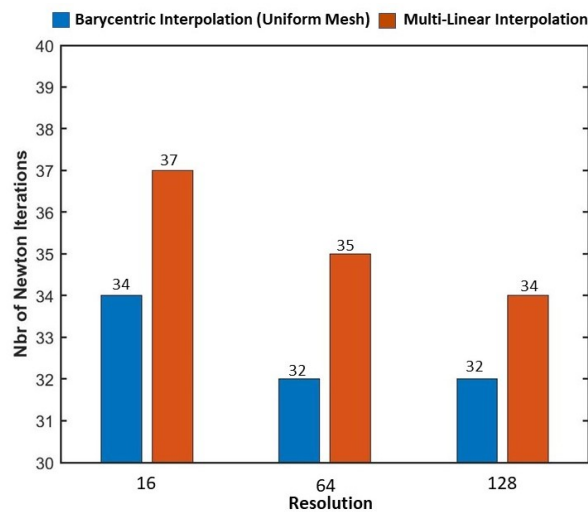


Figure 5.8: Number of Newton's iterations of barycentric interpolation with uniform mesh and multi-linear interpolation for Model 1 at Δt_{max} of 1 day

In the second model, a significant difference in iterations is observed at lower resolution. The difference in iterations between two methods is expected to grow when the simulation is performed with smaller timesteps.

5.5.2. Four Component System

With an increase in the number of components in the fluid system, higher resolutions are needed to model the compositional interaction between different components. The algorithm is flexible enough to accommodate a multicomponent system. The four component fluid

system of CO_2, C_1, nC_4, C_{10} considered. Pure CO_2 is injected at injector and mixture of light to intermediate hydrocarbons are produced at the producer. Maximum (Δt_{max}) of 0.9 days is taken for simulation.

Table 5.5: Injection and production conditions for 4 component fluid system

	p (bar)	CO_2	C_2	nC_4	C_{10}
Injection	100	0.97	0.01	0.01	0.01
Production	60	0.01	0.325	0.325	0.34

The results of 4 component system evidently prove that tie-simplex framework performs slightly better with multi-linear interpolation.

Constant K-values parametrization

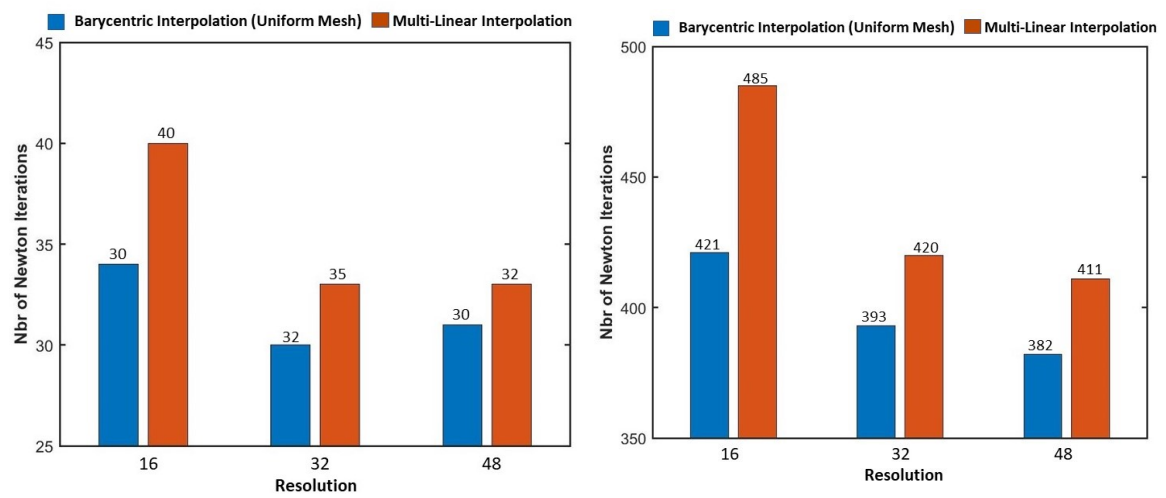


Figure 5.9: Number of Newton's iterations for multi-linear and tie-simplex parameterization for model 1(left) and model 2(right) for four component constant K values

EOS-based parametrization

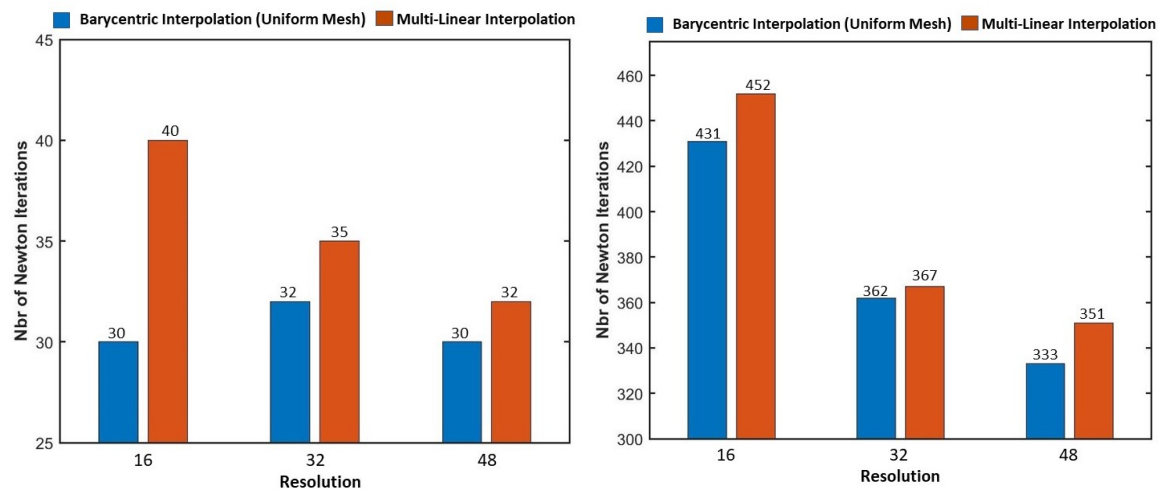


Figure 5.10: Number of Newton's iterations for barycentric interpolation and multi-linear interpolation for Model 1 (on left) and Model 2 (on right) for four component fully EOS case

5.6. Performance of Tie-Simplex Parameterization

Tie-simplex parameterization framework needs searching for a simplex corresponding to a query point from the tessellated space. This is computationally expensive with an increased number of components (dimensions), additionally, derivatives are calculated for every Newton's iteration until the end of the simulation. This increases interpolation time in tie-simplex framework considerably.

Instead, the constant derivative property is used to improve the interpolation speed. The derivatives of each simplex are determined during the initialization stage and stored in the form of objects at each pressure. During simulation, the unknowns $[p, z_i]$ obtained after every Newton's update gives query points. All the query points within each simplex are uniquely indexed and derivatives are extracted by accessing the objects stored earlier, without computing them during every iteration.

The comparison of interpolation time is mentioned below.

Table 5.6: Comparison of interpolation time of tie-simplex parameterization before and after initializing derivatives

Model	Resolution	Before Initialization	After Initialization
		(sec)	(sec)
Model 1	16	5.24	1.52
	64	9.9	2.80
	128	22.58	4.42
Model 2	16	136.2	83.6
	64	258.9	104.5
	128	408.7	129.2

This improves the computational efficiency of tie-simplex approach and thereby reducing the interpolation time by multifold. But due to searching criterion, multi-linear interpolation is still computationally effective since it bypasses the search for hypercube. But the true performance of interpolation has to be tested by integrating this framework into DARTS (Delft Advanced Research Terra Simulator).

6

Conclusions and Discussion

The main research objectives aimed to improve parameterization framework within Operator-Based Linearization approach is successively achieved. In chapter 2, a more accurate method of dealing with non-physical points within existing uniform parameterization is shown. Chapter 3 describes entirely new non-uniform parameterization framework. Delaunay method triangulates the non-uniformly scattered supporting points into simplexes and then these simplexes are tessellated as described in chapter. Operators are interpolated within each simplex by finding the barycentric coordinates of each vertex with respect to a query point. Interpolating query point is expressed as a linear combination of the vertex and its corresponding barycentric coordinate. The derivatives of operators to nonlinear unknowns are also determined through interpolation. Since the derivatives of interpolated operators does not change within a simplex, this inherent property helps to avoid calculation of derivatives at every query point in compositional space.

In chapter 4, it was shown how non-uniform parameterization can be built adaptively honoring underlying physics. A limited number of tie-lines are needed to fully parameterize the compositional space. The efficiency of the tie-simplex parameterization approach is also demonstrated successfully. This is done by finding the spatial distribution of errors in physical compositional space at different pressures. The operator values determined by multi-linear interpolation are taken as a reference for comparison. A maximum Euclidean error of accumulation and flux operator between adaptive parameterization and uniform parameterization validates the accuracy with tie-simplex approach.

Newly developed tie-simplex parameterization framework is then tested for a one-dimensional homogeneous transport solver (chapter 5). Here, the supporting points surrounding the solution path in parameter space take part in interpolation providing operator values along with derivatives to aid Jacobian assembly. The interpolation error accumulated over the simulation run compared for the two interpolation schemes for uniform and adaptive mesh. The applicability and efficiency of tie-simplex parameterization to the multicomponent system is demonstrated by comparison against uniform parameterization.

The key observations from this research are articulated below.

- For uniform parameterization of multicomponent system, the accuracy of interpolation performed close to non-physical domain of compositional space can be significantly improved by applying extrapolation technique.
- The computational cost of piece-wise multi-linear interpolation doubles with each new degree of freedom, making it difficult to apply to fluid systems with large number of components. Barycentric interpolation is more promising for such problems, because its performance drops much slower with growth of dimensionality, while values of derivatives remain constant for any query point within given simplex.

- Barycentric interpolation can be beneficial even if applied to uniform parameterization. First, it does not require parameterization of non-physical domain of compositional space. Second, the accuracy of barycentric interpolation is better than multi-linear interpolation simply because the size of interpolation body in barycentric interpolation is half of the one in multi-linear interpolation.
- The derivative of operators with respect to composition is constant within the simplex. So, there exists a discontinuity in derivative across every simplex, whereas a continuity in derivative is observed within a hypercube.
- Tie-lines are used as a basic reference for adaptive parameterization of compositional space. This approach allows to capture the phase boundary and minimize the error associated due to the nonlinear variation of the operator. Better accuracy is achieved at lower resolutions with adaptive mesh.
- Nonlinear Newton's solver experiences a faster convergence rate with barycentric interpolation, which performs better with the increase in dimensions, in comparison with multi-linear interpolation.
- Searching for the simplex corresponding to a query point is computationally demanding from n dimensional tessellation and this becomes more expensive with an increase in the degrees of freedom.

Recommendations

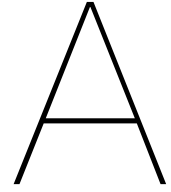
Tie-simplex parameterization framework has scope for improvement and further development. Possible research directions are briefly discussed below.

- Generalizing the adaptive parameterization developed for three component system to the multicomponent system.
- In the current parameterization approach, the variation of the operator along the tie-line is not considered. Operators vary along the tie-line and the change is significant close to phase boundary, this is due to the endpoint permeability induces the nonlinear behavior in operator close to the phase boundary, as shown in fig 4.12. While parameterizing, considering this variation along the tie-line will bring robustness to this approach by further increases the accuracy and reducing the error around phase boundary.
- The robustness and efficiency of tie-simplex parameterization framework should be tested by including buoyancy forces and capillary pressure effects.
- In order to assess the effect of adaptive mesh on nonlinear Newton's solver, test cases of immiscible and miscible displacement should be considered and a convergence study on this will provide more insights on the behavior of Newton solver.
- Integrating and testing the performance of interpolation in DARTS (Delft Advanced Research Terra Simulator). If the performance is affected due to search criterion in n -dimensional tessellation, then optimization simplex strategy proposed by Nelder and Mead (1965) should be tried as a search criterion.
- Due to the hyperbolic nature of the problem, the solution path covers only a small portion of parameter space, leaving a certain portion of parameter space unused. This unused parameter space grows exponentially with an increase in the degrees of freedom. Using tie-simplex approach, only a subset of entire parameter space between injection and production condition is parameterized. This can help to make a pre-processing stage faster and facilitates running higher resolution at the same computational expense.

Bibliography

- Gabor Acs, Sandor Doleschall, Eva Farkas, et al. General purpose compositional model. *Society of Petroleum Engineers Journal*, 25(04):543–553, 1985.
- K Aziz and TW Wong. Considerations in the development of multipurpose reservoir simulation models. In *proceedings of the 1st and 2nd International Forum on Reservoir Simulation, Alpbach, Austria*, 1989.
- Khalid Aziz. Petroleum reservoir simulation. *Applied Science Publishers*, 476, 1979.
- JD Bolling et al. Development and application of a limited-compositional, miscible flood reservoir simulator. In *SPE Symposium on Reservoir Simulation*. Society of Petroleum Engineers, 1987.
- John Charles Butcher. *Numerical methods for ordinary differential equations*. John Wiley & Sons, 2016.
- Keith H Coats et al. An equation of state compositional model. *Society of Petroleum Engineers Journal*, 20(05):363–376, 1980.
- Boris Delaunay et al. Sur la sphere vide. *Izv. Akad. Nauk SSSR, Otdelenie Matematicheskii i Estestvennyka Nauk*, 7(793-800):1–2, 1934.
- VM Entov, FD Turetskaya, and DV Voskov. On approximation of phase equilibria of multi-component hydrocarbon mixtures and prediction of oil displacement by gas injection. In *ECMOR VIII-8th European Conference on the Mathematics of Oil Recovery*, 2002.
- Øivind Fevang, Kameshwar Singh, Curtis H Whitson, et al. Guidelines for choosing compositional and black-oil models for volatile oil and gas-condensate reservoirs. In *SPE annual technical conference and exhibition*. Society of Petroleum Engineers, 2000.
- Schlumberger GeoQuest. Eclipse reservoir simulator. *Technical description*, 2009.
- Alireza Iranshahr, Denis Voskov, Hamdi A Tchelepi, et al. Tie-simplex parameterization for eos-based thermal compositional simulation. *SPE Journal*, 15(02):545–556, 2010.
- M Khait, D Voskov, and G Konidala. Tie-simplex parametrization for operator-based linearization for non-isothermal multiphase compositional flow in porous. In *ECMOR XVI-16th European Conference on the Mathematics of Oil Recovery*, 2018a.
- Mark Khait and Denis Voskov. Operator-based linearization for efficient modeling of geothermal processes. *Geothermics*, 74:7–18, 2018.
- Mark Khait and DV Voskov. Operator-based linearization for modeling of low-enthalpy geothermal processes. 2016.
- Mark Khait, Denis Voskov, et al. Adaptive parameterization for solving of thermal/compositional nonlinear flow and transport with buoyancy. *SPE Journal*, 2018b.
- Narayana Rao Nagarajan, Mehdi Matt Honarpour, Krishnaswamy Sampath, et al. Reservoir fluid sampling and characterization—key to efficient reservoir management. In *Abu Dhabi International Petroleum Exhibition and Conference*. Society of Petroleum Engineers, 2006.
- John A Nelder and Roger Mead. A simplex method for function minimization. *The computer journal*, 7(4):308–313, 1965.

- Franklin Mattes Orr et al. *Theory of gas injection processes*, volume 5. Tie-Line Publications Copenhagen, 2007.
- Ding-Yu Peng and Donald B Robinson. A new two-constant equation of state. *Industrial & Engineering Chemistry Fundamentals*, 15(1):59–64, 1976.
- HH Rachford Jr, JD Rice, et al. Procedure for use of electronic digital computers in calculating flash vaporization hydrocarbon equilibrium. *Journal of Petroleum Technology*, 4(10):19–3, 1952.
- Vaclav Skala. Barycentric coordinates computation in homogeneous coordinates. *Computers and Graphics (Pergamon)*, 2008. ISSN 00978493. doi: 10.1016/j.cag.2007.09.007.
- Denis Voskov, Hamdi A Tchelepi, et al. Compositional space parameterization for flow simulation. In *SPE Reservoir Simulation Symposium*. Society of Petroleum Engineers, 2007.
- Denis V. Voskov. Operator-based linearization approach for modeling of multiphase multi-component flow in porous media. *Journal of Computational Physics*, 2017. ISSN 10902716. doi: 10.1016/j.jcp.2017.02.041.
- Denis V. Voskov and Hamdi A. Tchelepi. Tie-simplex based mathematical framework for thermodynamical equilibrium computation of mixtures with an arbitrary number of phases. *Fluid Phase Equilibria*, 2009. ISSN 03783812. doi: 10.1016/j.fluid.2009.04.018.
- Denis V Voskov, Hamdi A Tchelepi, et al. Compositional space parameterization: theory and application for immiscible displacements. *SPE Journal*, 14(03):431–440, 2009a.
- Denis V Voskov, Hamdi A Tchelepi, et al. Compositional space parameterization: Multi-contact miscible displacements and extension to multiple phases. *SPE Journal*, 14(03): 441–449, 2009b.
- Joe Warren, Scott Schaefer, Anil N Hirani, and Mathieu Desbrun. Barycentric coordinates for convex sets. *Advances in computational mathematics*, 27(3):319–338, 2007.
- Rustem Zaydullin, Denis Voskov, Hamdi A Tchelepi, et al. Nonlinear formulation based on an equation-of-state free method for compositional flow simulation. *SPE Journal*, 18(02): 264–273, 2012.
- Rustem Zaydullin, DV Voskov, HA Tchelepi, et al. Formulation and solution of compositional displacements in tie-simplex space. In *SPE Reservoir Simulation Symposium*. Society of Petroleum Engineers, 2013.



Appendix 1

Algorithm

A brief overview of the algorithm for Tie-simplex interpolation is mentioned below.

1. Step 1 - Pre Processing Stage

- Parameterizing the space uniformly (or) using tie-simplex approach.
- The Supporting points obtained from parameterization are used to calculate the operator values α and β . The results are stored in multi-dimensional tables. Number of tables generated depends on the composition. Each operator needs n_c number of tables corresponding to each composition.

2. Step 2 - Initialization Stage

- Reading the tables which contain the supporting points with the operator values.
- Tessellating the compositional space for every pressure using delaunay triangulation.
- Extracting the vertices of simplex and corresponding composition for finding derivatives within each simplex.
- Saving the interpolant function and the derivatives of each simplex in terms of objects for further accessing during simulation.

3. Step 3- Interpolating operators

- Extracting the query points $[p, z_1, \dots, z_{n_c-1}]$ which lies between every successive pressure interval along the pressure axis.
- Finding out the interpolant function corresponding to lower and upper pressure from previously saved objects.
- Interpolating the operator in the composition planes belonging to lower and upper bound pressure, and finding the weights of the query point located between two pressure planes $[P_i, P_{i+1}]$

$$w = \frac{p - P_i}{P_{i+1} - P_i}$$

4. Step 4- Finding derivatives

- Locating the simplex within which the query point lies in the composition plane of upper and lower bound pressure.
- Picking the derivative of operator of that particular simplex in both the composition planes
- Interpolating the derivative $\frac{df}{dz}$ of the query point by finding the weights as mentioned above.

B

Appendix 2

B.1. Rock and fluid properties for OBL

Below are the input reservoir properties considered for running OBL framework.

Table B.1: Rock and fluid properties considered for OBL framework

Property	Notation	Value	Units
Porosity	Φ	0.2	-
Permeability	K	100	mD
Rock Compressibility	c_r	10^{-7}	1/bar
Residual saturation	S_{rj}	0	-
Corey exponent	n	2	-
Lower pressure limit	p_{min}	20	bar
Upper pressure limit	p_{max}	130	bar

B.2. Inputs of 1D reservoir simulation model

1D transport solver is used for validating the tie-simplex and comparing newton convergence criterion with multi-linear interpolation. The input parameters for the results presented in ??.

Table B.2: Inputs parameters for 1D system for three and four component system

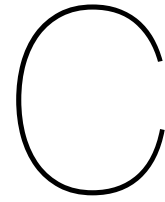
Property	Value	Units
Model 1	100 blocks	-
Model 2	500 blocks	-
Initial time step	$\Delta t_{max}/16$	days
Maximum newton iterations	40	-
Injection Pressure	100	bar
Initial Pressure	60	bar

Table B.3: Input parameters for 1D simulation

components	Inputs	Model 1		Model 2	
		Constant K	EOS	Constant K	EOS
3 Components	Resolution	16,64,128	16,64,128	16,64,128	16,64,128
	Maximum Time step (Δt_{max})	0.2 days	0.2 days	0.2 days	0.2 days
	Total simulation time	4.5 days	4.5 days	120 days	120 days
4 Components	Resolution	16,32,48	16,32,48	16,32,48	16,32,48
	Maximum Time step (Δt_{max})	0.9 days	0.9 days	0.9 days	0.9 days
	Total simulation time	2.5 days	2.5 days	90 days	80 days

Table B.4: K values for three and four component system

Number of components	Components	K values
3	C_{O_2}, nC_4, C_{10}	[3, 1.5, 0.05]
4	$C_{O_2}, C_1, nC_4, C_{10}$	[1.5, 2.5, 0.5, 0.05]



Appendix 3

C.1. Geometric Constraint at Low Pressures

The ternary representation with parameterization is shown in the image below. Blue dots are the supporting points resulted from the adaptive construction.

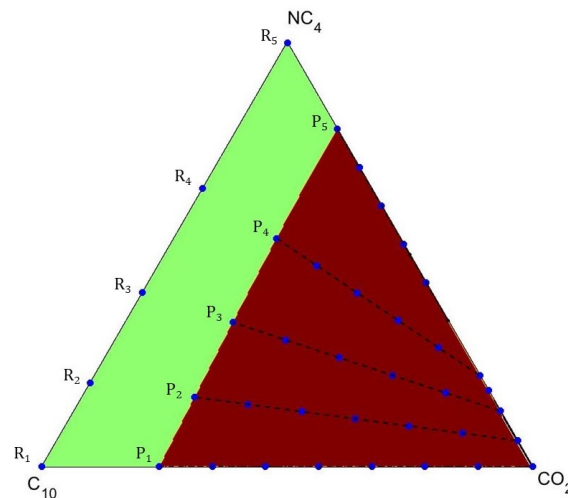


Figure C.1: Ternary representation of parameterization scheme for 20 bar pressure

As we see, the distance between P_4, P_5 is more compared to the distance between the remaining any two successive tie lines. The constructed mesh from Delaunay triangulation is bigger in this region, which can be seen in the error plot of α at the same pressure, below. The error due to this constraint is visible in accumulation term because at low pressure because of α is relative less nonlinear compared to flux which is highly nonlinear around phase boundary.

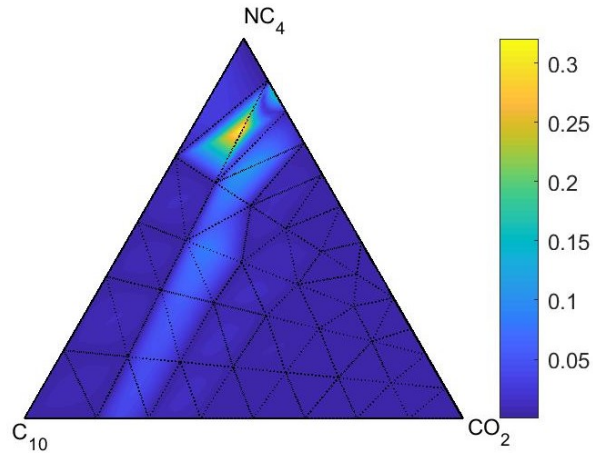


Figure C.2: Ternary representation of parameterization scheme for 20 bar pressure

C.2. Derivatives Plots at Higher Resolution

For three component fluid system, at 60 bar pressure, the derivative plots of α and β w.r.t unknowns are presented below, at high resolution (100 x 100).

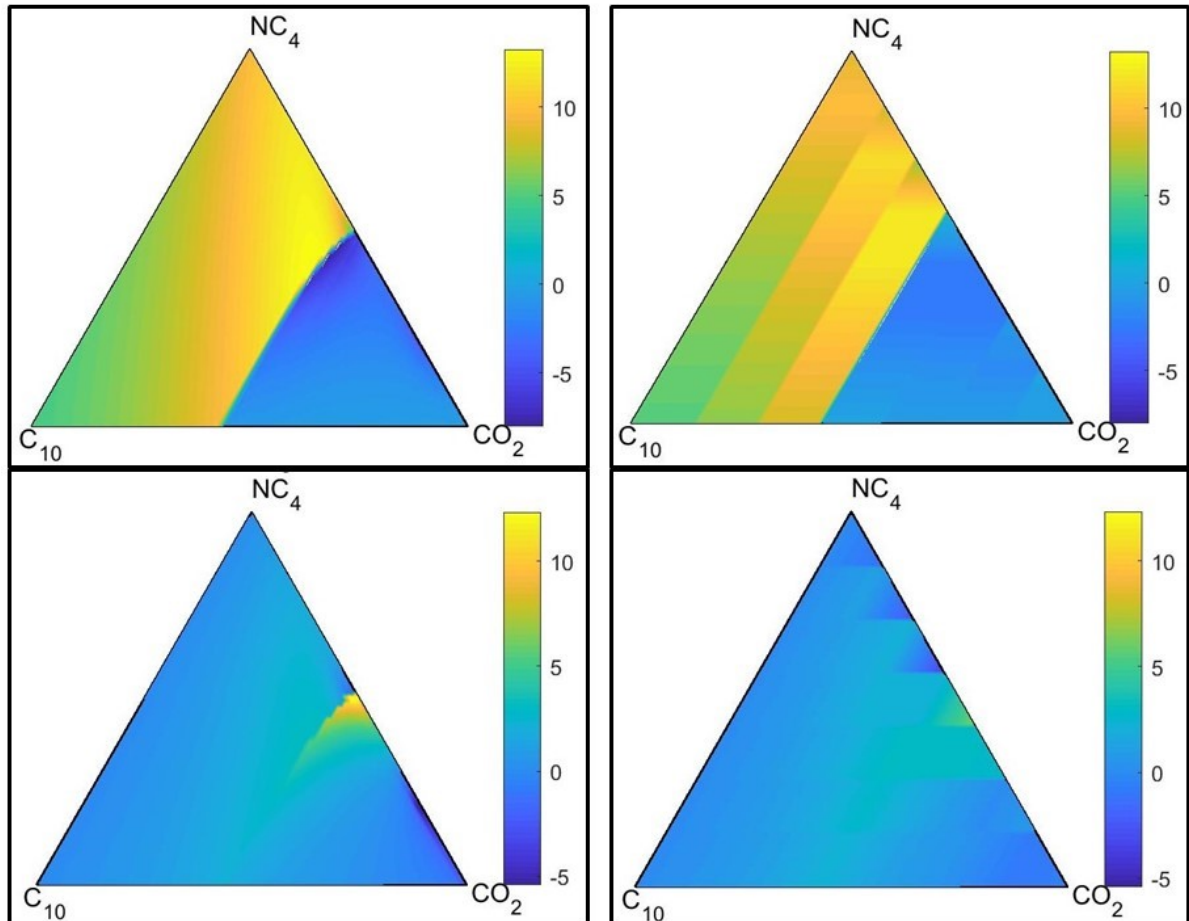


Figure C.3: Derivatives of α about z_1 (on top) and about z_2 (bottom) using tie-simplex (left) and multi-linear (right) interpolation for Fully EOS case at resolution 100

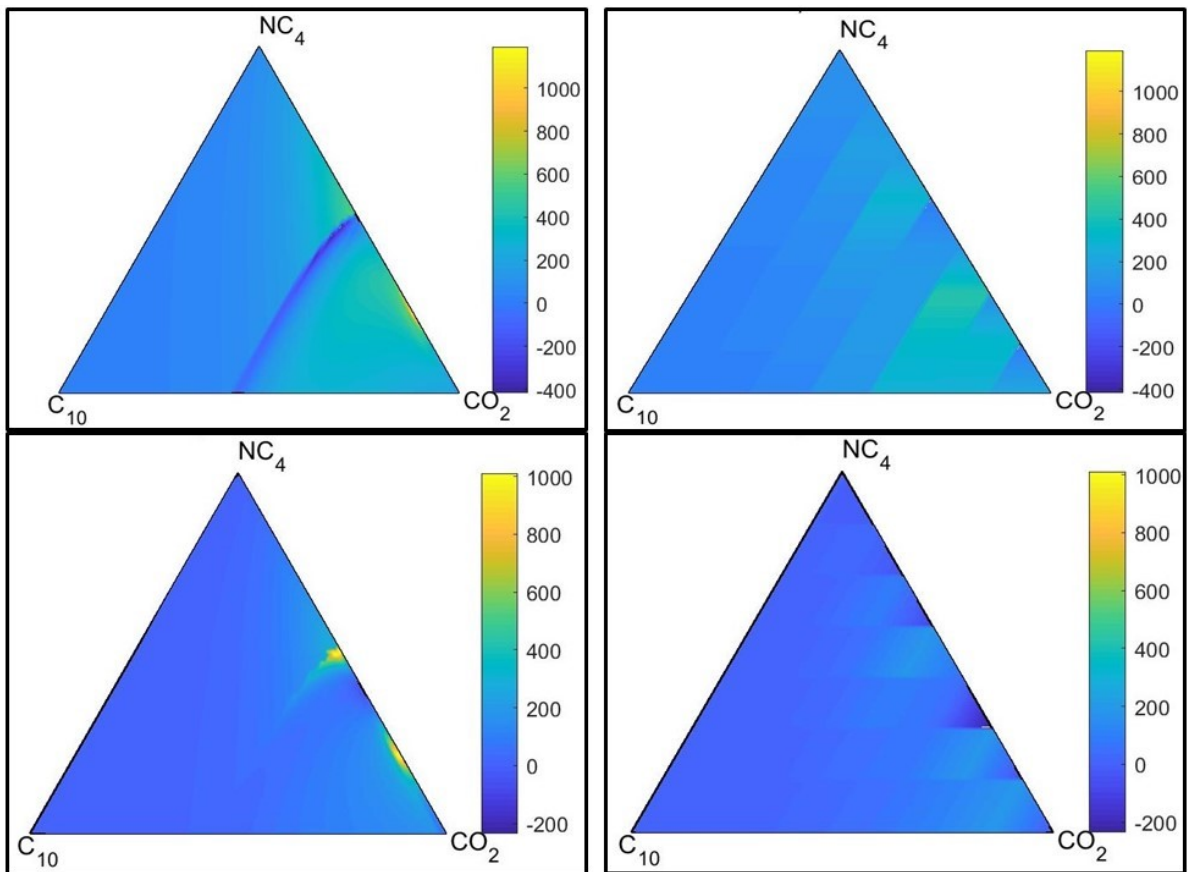


Figure C.4: Derivatives of β about z_1 (on top) and about z_2 (bottom) using tie-simplex (left) and multi-linear (right) interpolation for fully EOS case at resolution 100